Interfaces Free Bound. 28 (2026), 463–500
DOI 10.4171/IFB/559

© 2026 European Mathematical Society
Published by EMS Press
This work is licensed under a CC BY 4.0 license

A penalized Allen–Cahn equation for the mean curvature flow of thin structures

Elie Bretin, Chih-Kang Huang, and Simon Masnou

Abstract. This paper addresses the approximation of the mean curvature flow of thin structures for which classical phase field methods are not suitable. By thin structures, we mean surfaces that are not domain boundaries, typically higher codimension objects such as 1D curves in 3D—that is, filaments, or soap films spanning a boundary curve. To approximate the mean curvature flow of such surfaces, we consider a small thickening and we apply to the thickened set an evolution model that combines the classical Allen–Cahn equation with a penalty term that takes on larger values around the skeleton of the set. The novelty of our approach lies in the definition of this penalty term that guarantees a minimal thickness of the evolving set and prevents it from disappearing unexpectedly. We prove a few theoretical properties of our model, provide examples showing the connection with higher codimension mean curvature flow, and introduce a quasi-static numerical scheme with explicit integration of the penalty term. We illustrate the numerical efficiency of the model with accurate approximations of filament structures evolving by mean curvature flow, and we also illustrate its ability to find complex 3D approximations of (at least local) solutions to the Steiner problem or the Plateau problem.

1. Introduction

The aim of this paper is to introduce a model and a numerical method for approximating the evolution of thin structures via mean curvature flow. As a specific example of thin structures, we focus on filaments in 3D space, which are typical codimension 2 objects possibly with singularities. The method we introduce is actually suitable for more general structures, such as surfaces which are not domain boundaries. It is therefore relevant to various physical applications, as we illustrate with numerical approximations of (at least local) solutions to the Steiner or Plateau problems in 3D.

The evolution by mean curvature of thin structures such as filaments falls into the category of higher codimension mean curvature flows, that is, mean curvature flows of submanifolds with codimension at least 2. A first list of references (see [10]) for the definition, the analysis, and the approximation of higher-codimension flows is [2, 6, 7, 11, 13, 33, 58, 63]; see also [42, 46, 61], the survey paper [59], and the references therein.

Mathematics Subject Classification 2020: 53E10 (primary); 35A35, 65M22, 35A15, 53A07 (secondary).
Keywords: phase field approximation, mean curvature flow, thin structures, higher codimension, skeleton, Steiner problem, Plateau problem, numerical approximation.

Various methods have been proposed to approximate numerically these flows. The curve shortening flow in higher codimension was for example approximated numerically with finite elements in [8, 9, 34, 36, 38], with a semi-Lagrangian scheme and a level set approach in [24] (for codimension 2 curves), and with a parametric approach in [48]. Finite elements were also used for approximating the anisotropic curve shortening [51] or the mean curvature flow of surfaces in arbitrary codimension [14, 52]. Bence–Merriman–Osher-type algorithms have been introduced and studied to approximate codimension 2 mean curvature flows; see, for instance, [45, 55]. Recently, a method based on neural networks was proposed in [22] to handle the mean curvature motion of a large variety of objects: oriented and non-oriented curves or surfaces, curve networks, multiphase systems, and curves or surfaces with boundary constraints, with applications to the Steiner or Plateau problems.

In general, the above numerical approaches are not as effective as their counterparts designed for codimension 1 surfaces, with the notable exception of [22], which seems very well suited to extensions to higher codimension (see also the recent contribution [20] where a phase field approximation of non-oriented interfaces is introduced).

In this paper, we address this limitation by showing how classical phase field methods can be used to approximate, at least formally, the mean curvature flow of higher codimension interfaces, possibly associated with boundary constraints. This is achieved considering the mean curvature motion of tubular neighborhoods of the interfaces, combined with implicit thickness constraints.

1.1. Classical mean curvature flow and its phase field approximation

The classical mean curvature flow starting from a smooth open set $\Omega \subset \mathbb{R}^N$ is a time-dependent set $\Omega(t)$ whose inner normal velocity $V_n(x)$ at each point x of $\partial\Omega(t)$, as long as it can be defined, is proportional to the scalar mean curvature $H_{\partial\Omega(t)}(x)$. Here, we use the sign convention that the scalar mean curvature of a convex surface is non-negative. Up to time rescaling, the evolution flow takes the form

$$V_n(x) = H_{\partial\Omega(t)}(x), \quad x \in \partial\Omega(t),$$

which corresponds to the evolution of $\partial\Omega(t)$ by the L^2-gradient flow of the perimeter

$$P(\Omega(t)) = \mathcal{H}^{N-1}(\partial\Omega(t)),$$

where $\mathcal{H}^{N-1}$ is the $(N-1)$-Hausdorff measure.

This emblematic geometric flow has been the subject of extensive research; see [10] and the references therein. To deal with singularities, which can develop in finite time and mark the limit of existence of the smooth flow, various notions of weak mean curvature flows have been introduced; see, for example, the references in [5, 10, 41, 46, 61]. The approximation of mean curvature flow has been addressed with various models and numerical methods, particularly parametric, level set, convolution-thresholding, or phase

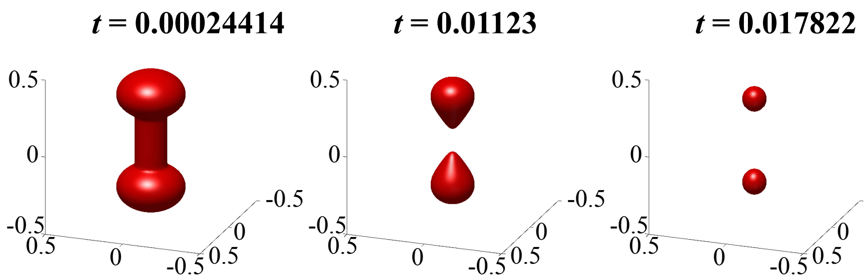

Figure 1. Phase field approximation beyond singularities of the mean curvature flow of a dumbbell.

field approaches; see [3] for a theoretical perspective on some of these approaches. It is worth emphasizing that a wider class of singularities can be handled by the last three methods; see an example in Figure 1.

In the theory of phase field approximation, the fundamental work of Modica and Mortola [49] showed that the perimeter of a set can be approximated in the sense of Γ convergence (for the L^1 topology) by the smooth Van der Waals–Cahn–Hilliard energy

$$P_\varepsilon(u) = \int_Q \left(\frac{\varepsilon}{2}|\nabla u|^2 + \frac{1}{\varepsilon}W(u)\right) dx.$$

where $Q \subset \mathbb{R}^N$ is a sufficiently large fixed bounded domain, $\varepsilon > 0$ is a small parameter and W is a smooth double-well potential, typically

$$W(s) = \frac{1}{2}s^2(1-s)^2.$$

In particular, the characteristic function of a set Ω of finite perimeter can be approximated in L^1 by functions of the form $u_\varepsilon = q(\frac{\mathrm{dist}(x,\Omega)}{\varepsilon})$ so that $P_\varepsilon(u_\varepsilon) \to c_W P(\Omega)$ as $\varepsilon \to 0$, with $c_W = \int_0^1 \sqrt{2W(s)}ds$. Here, $q(s) = \frac{1}{2}(1-\tanh(s/2))$ is an optimal profile associated with the above choice of W, that is, a minimizer of the associated 1D Van der Waals–Cahn–Hilliard energy with suitable values at $\pm\infty$ and 0, and $\mathrm{dist}(\cdot,\Omega)$ is the signed distance function to Ω with the convention that $\mathrm{dist}(\cdot,\Omega)$ takes negative values in the interior of Ω and positive values outside.

The L^2-gradient flow of the Van der Waals–Cahn–Hilliard energy P_ε results in the Allen–Cahn equation [1], that is, up to a time rescaling,

$$u_t = \Delta u - \frac{1}{\varepsilon^2}W'(u). \tag{1.1}$$

The Cauchy problem for this non-linear parabolic equation has a unique solution that satisfies a comparison principle; see, for instance, [3, Chap. 14]. Furthermore, a smooth set Ω evolving by mean curvature flow can be approximated by

$$\Omega^\varepsilon(t) = \left\{x \in \mathbb{R}^N,\ u^\varepsilon(x,t) \geq \frac{1}{2}\right\},$$

where u^ε solves (1.1) with initial condition

$$u^\varepsilon(x,0) = q\Big(\frac{\operatorname{dist}(x,\Omega(0))}{\varepsilon}\Big).$$

A formal asymptotic expansion of u^ε near the interfaces [10] shows that u^ε is quadratically close to the optimal profile, that is,

$$u^\varepsilon(x,t) = q\Big(\frac{\operatorname{dist}(x,\Omega^\varepsilon(t))}{\varepsilon}\Big) + O(\varepsilon^2),$$

and the inner normal velocity V^ε of the interface $\{u^\varepsilon = \frac{1}{2}\}$ satisfies

$$V^\varepsilon = H + O(\varepsilon^2).$$

The convergence of $\partial\Omega_\varepsilon(t)$ to $\partial\Omega(t)$ as $\varepsilon \to 0$ has been rigorously proved for smooth flows in [12, 28, 32] with a quasi-optimal convergence order $O(\varepsilon^2|\log\varepsilon|^2)$. The fact that u^ε is quadratically close to the optimal profile has inspired the development of very effective numerical methods in [19, 54, 60].

1.2. Mean curvature flow of thin tubular sets and thickness constraint

Let Σ denote a set of codimension at least 2. If it is smooth, its vector mean curvature H_Σ is well defined, and therefore the classical motion of Σ by mean curvature, characterized by the (vector) velocity $V = H_\Sigma$ at each point, is well defined locally in time. To approximate this higher codimension mean curvature flow, the central idea of this paper is to consider a σ-neighborhood Σ_σ of Σ, and a phase field mean curvature motion of this neighborhood with a control of its thickness to prevent its disappearance or any topological change. There are classical theoretical approaches to the higher codimension mean curvature flow that involve either phase field methods or tubular neighborhoods (see, e.g., [6, 7, 11, 13]), but they are difficult to approximate numerically, in contrast to our model, as will be shown later. In practice, we consider the perturbed Allen–Cahn equation

$$\partial_t u^\varepsilon = \Delta u^\varepsilon - \frac{W'(u^\varepsilon)}{\varepsilon^2}(1 + f^\sigma), \tag{1.2}$$

where the forcing term f^σ acts as a Lagrange multiplier associated with an implicit constraint that the thickness of the evolving domain is bounded from below by σ.

As we will see, the sharp interface limit of this equation gives the following law at the boundary of Σ_σ:

$$V_n = H - \frac{\nabla f^\sigma \cdot n}{2(1 + f^\sigma)},$$

where n is the inner unit normal on $\partial\Sigma_\sigma$, V_n is the scalar normal velocity, and H is the scalar mean curvature.

The main difficulty with the above model lies in identifying a suitable definition for the forcing term f^σ. To address this, we exploit the properties of the signed distance function and the asymptotic expansion of the solutions to the Allen–Cahn equation, which allow us to identify the skeleton of Σ_σ, taken as an approximation of Σ. This analysis leads us to the following definition of f^σ:

$$f^\sigma = c(h^\sigma * |\langle n^\sigma_{u^\varepsilon}, (\nabla n^\sigma_{u^\varepsilon})^T n^\sigma_{u^\varepsilon}\rangle|),$$

where $c > 0$ is a constant and $n^\sigma_{u^\varepsilon} = h^\sigma * \frac{\nabla u^\varepsilon}{|\nabla u^\varepsilon|}$, with h^σ a smoothing kernel, typically a Gaussian kernel of standard deviation σ.

We provide in the following both theoretical and numerical arguments to show that such a forcing term is primarily active near the skeleton of Σ_σ and, in practice, serves to both locate the skeleton and maintain a minimum distance of σ between $\partial\Sigma_\sigma$ and the skeleton throughout the flow. The initialization of our flow involves computing a distance function; however, in contrast with level set methods, our approach does not require redistancing at every iteration. In particular, the characterization of the skeleton is solely based on the computation of the forcing term f^σ, which eliminates the need for repeated redistancing and avoids the inaccuracies typically associated with the classical level set numerical discretization of mean curvature flow.

We will provide theoretical and numerical arguments showing the connection of our modified Allen–Cahn equation with the (higher codimension) mean curvature flow of Σ. In particular, our approach provides an accurate numerical approximation of the mean curvature flow of tubular sets, possibly with endpoints constraints as in the Steiner problem. We will also illustrate that our model can be extended to approximate solutions to the Plateau problem, even in the case where the solution is not orientable. This proves the versatility of our method and its ability to handle complex geometric problems.

1.3. Outline of the paper

The paper is organized as follows:

In Section 2, we consider a forced mean curvature flow of a domain Ω with normal velocity $V_n = H + g$. We show that, being appropriately chosen, a forcing term g can prevent the boundary $\partial\Omega$ from approaching a fixed set Σ of codimension 2.

Section 3 is devoted to identifying implicitly the skeleton of Ω by exploiting the properties of its signed distance function. To address this, we use an approximation of the term

$$Sn = \langle n, \nabla n^T n\rangle,$$

where n is the gradient of the distance function.

In Section 4, we discuss a quasi-static numerical discretization of the perturbed Allen–Cahn equation (1.2). The section ends with numerical experiments that illustrate the ability of our approach to model accurately the evolution by mean curvature of filaments.

Lastly, in Sections 5 and 6, we explain how to couple the perturbed equation with additional inclusion constraints. We deduce numerical approximations of (at least local) solutions in 3D to the Steiner problem and to the Plateau problem, using for the latter a penalization of the volume. Of course, since our method is derived from a gradient flow, we cannot guarantee theoretically that it converges to global minimizers—it rather provides local minimizers. We observe, however, that the numerical solutions we obtain in several classical situations are perfectly consistent with known exact minimizers.

2. Approximation of the mean curvature flow with thin fixed obstacles

Given a closed obstacle $\Sigma \subset \mathbb{R}^N$ (typically a closed Lipschitz set possibly with boundary, but some results proved below remain true for more general sets), the aim of this section is to study how the classical Allen–Cahn equation can be modified to approximate the evolution by mean curvature of the boundary of a smooth bounded open set Ω constrained to remain at a distance not smaller than σ from Σ.

2.1. Motivations

We assume in the following that the obstacle Σ is contained in the interior of a smooth open set Ω with a distance from $\partial\Omega$ at least equal to $\sigma > 0$. The case where it is contained in the complementary of Ω can be considered in a similar way. We begin by proving that, the distance from Σ to $\partial\Omega$ being positive, the mean curvature at the point of $\partial\Omega$ closest to Σ is bounded from above. This result is essential since, if we consider the mean curvature flow with a forcing term g, that is, $V_n = H + g$, it is possible to choose g large enough near Σ to be sure that it prevents $\partial\Omega$ from flowing closer to Σ. Moreover, choosing g such that it takes values close to 0 far from Σ makes it almost inactive there, so that the constrained flow of $\partial\Omega$ far from Σ is very close to the classical mean curvature flow.

Lemma 2.1. *Let $\Sigma \subset \mathbb{R}^N$ be a closed set, and $\Omega \subset \mathbb{R}^N$ an open, bounded set with C^2 boundary such that* $\operatorname{dist}(\partial\Omega, \Sigma) = \delta > 0$. *Let $s_0 \in \partial\Omega$ be such that* $\operatorname{dist}(s_0, \Sigma) = \operatorname{dist}(\partial\Omega, \Sigma)$. *Then*

$$H_\Omega(s_0) \le \frac{N-1}{\delta}.$$

Proof. There exists a point $p \in \Sigma$ such that $\operatorname{dist}(s_0, \Sigma) = \|s_0 - p\| = \delta > 0$. Up to some linear transformation on $\mathbb{R}^N$, we can assume that p has coordinates $(0_{\mathbb{R}^{N-1}}, \delta)$, s_0 has coordinates $(0_{\mathbb{R}^{N-1}}, 0)$, and the interface $\partial\Omega$ can be locally considered as the graph of a regular function $\psi : V \subset \mathbb{R}^{N-1} \to \mathbb{R}$ defined on a neighborhood V of $0_{\mathbb{R}^{N-1}}$ such that $\psi(0_{\mathbb{R}^{N-1}}) = 0$ and $\nabla\psi(0_{\mathbb{R}^{N-1}}) = 0_{\mathbb{R}^{N-1}}$. Therefore, the scalar mean curvature of $\partial\Omega$ at

$s_0 = (0_{\mathbb{R}^{N-1}}, 0)$ is

$$H_\Omega(s_0) = \operatorname{div}\Big(\frac{\nabla\psi}{\sqrt{1+|\nabla\psi|^2}}\Big)(0_{\mathbb{R}^{N-1}}) = \Delta\psi(0_{\mathbb{R}^{N-1}})$$

and we have that

$$\psi(x) = \frac{1}{2}\langle x, \nabla^2\psi(0_{\mathbb{R}^{N-1}})x\rangle + o(\|x\|^2), \qquad \text{as } x \to 0. \tag{2.1}$$

Thanks to the definition of δ, for all x in a neighborhood of $0_{\mathbb{R}^{N-1}}$,

$$\|x - 0_{\mathbb{R}^{N-1}}\|^2 + (\psi(x) - \delta)^2 \geq \delta^2,$$

which gives

$$\|x\|^2 - 2\delta\psi(x) + \psi(x)^2 \geq 0.$$

Hence, by considering $x = \epsilon e_j$ where $(e_1, \dots, e_{N-1})$ is the canonical basis of $\mathbb{R}^{N-1}$and by dividing the above inequality by ϵ^2, as ϵ goes to 0, thanks to (2.1), we obtain that

$$\delta(\nabla^2\psi(0))_{jj} \leq 1,$$

which leads to

$$H_\Omega(s_0) = \sum_{j=1}^{N-1}(\nabla^2\psi(0))_{jj} \leq \frac{N-1}{\delta}. \qquad \blacksquare$$

2.2. The Allen–Cahn equation with a forcing term

A classical perturbation of the Allen–Cahn equation consists in adding a forcing term g^ε and considering

$$\partial_t u^\varepsilon = \Delta u^\varepsilon - \frac{W'(u^\varepsilon)}{\varepsilon^2} + g^\varepsilon.$$

When the forcing term g^ε satisfies

$$\sup_{\varepsilon>0}\int_0^T \int \varepsilon g^\varepsilon(x,t)dxdt < +\infty,$$

Mugnai and Röger proved in [50] that the above phase field model converges to a forced mean curvature flow (in the sense of varifolds) with vector velocity

$$V = H + g,$$

where H is the vector mean curvature and g a vector field characterized by

$$\lim_{\varepsilon\to 0}\int_0^T \int_{\mathbb{R}^N} \eta \cdot \nabla u^\varepsilon g^\varepsilon \, dx\, dt = \int_0^T \int_{\mathbb{R}^N} \eta \cdot g \, d\mu,$$

for every $\eta \in C_c^0((0,T)\times\mathbb{R}^N,\mathbb{R}^N)$. Here μ is a Radon measure on $(0,T)\times\mathbb{R}^N$ obtained as the limit of the *diffuse surface area measures*

$$\mu^\varepsilon := \Big(\frac{\varepsilon}{2}|\nabla u^\varepsilon|^2 + \frac{1}{\varepsilon}W(u^\varepsilon)\Big)\mathcal{L}^{N+1}.$$

Recall that the Allen–Cahn equation is, up to a rescaling of time, the L^2-gradient flow of the Cahn–Hilliard energy P_ε. The Allen–Cahn equation combined with the forcing term g^ε can be obtained, with the same rescaling of time, as the gradient of

$$P_\varepsilon + \varepsilon\int_{\mathbb{R}^N} g^\varepsilon u^\varepsilon dx.$$

However, the additional penalty term is not well suited to our problem, as it penalizes the whole interior of Ω^ε (see [23]) and not only the interface $\partial\Omega^\varepsilon$. An easy way to focus on the boundary of Ω^ε is to use a weight of the form $W(u^\varepsilon)$, which is active only near $\partial\Omega^\varepsilon$, along with a penalty term of the form

$$\frac{1}{\varepsilon}\int_\Sigma W(u^\varepsilon(x,t))d\mathcal{H}^k(x),$$

assuming that Σ is a k-dimensional set. A diffuse approximation of this penalty term is

$$\frac{1}{\varepsilon}\int_{\mathbb{R}^N} f^\sigma(x)W(u^\varepsilon(x,t))dx,$$

where $f^\sigma dx$ is a non-negative smooth approximation of $\mathcal{H}^k \llcorner \Sigma$. Such a penalty term leads to the perturbed Allen–Cahn equation

$$\partial_t u^\varepsilon = \Delta u^\varepsilon - \frac{W'(u^\varepsilon)}{\varepsilon^2}(1+f^\sigma),$$

which has been studied by Qi and Zheng in [53]. In particular, it is proved in [53] that if $1+f^\sigma > 0$, then the sharp interface limit of the equation corresponds to a forced mean curvature flow in the sense of varifolds with a vector motion law given by

$$V = H - \frac{\nabla^\perp f^\sigma}{2(1+f^\sigma)}, \tag{2.2}$$

where $\nabla^\perp f^\sigma$ is obtained from ∇f^σ by removing its tangential component.

We will now discuss the behavior of the forcing term in (2.2) and prove that, under certain conditions on f^σ, (2.2) provides a flow with obstacle.

2.3. Choosing the forcing term

We define f^σ as the Lebesgue density of the convolution of $\mathcal{H}^k \llcorner \Sigma$ with the Gaussian kernel

$$h^\sigma(x) = \frac{1}{\sigma^N}e^{-\frac{|x|^2}{\sigma^2}},$$

which provides a natural approximation of $\mathcal{H}^k \llcorner \Sigma$. Let us examine the consequences of this choice.

2.3.1. Case where Σ is a single point. We first consider the simplest case where $\Sigma = \{0\}$ and the forcing term f^σ is defined by

$$f^\sigma(x) = \delta_0 * h^\sigma(x) = \frac{1}{\sigma^N} e^{-\frac{|x|^2}{\sigma^2}}.$$

Lemma 2.2. *To any* $0 < \sigma < 1$, *we associate the function* $f^\sigma(x) = \sigma^{-N} e^{-\frac{|x|^2}{\sigma^2}}$. *For all* $0 < \sigma < \exp(\frac{2(1-N)}{N})$, *there exists an interval* I_σ *containing* $\sigma\sqrt{-N \ln \sigma}$ *such that, for every open bounded set* $\Omega \ni 0$ *with smooth boundary and satisfying* $\operatorname{dist}(0, \partial\Omega) = \delta > 0$ *with* $\delta \in I_\sigma$, *and for* $s_0 \in \partial\Omega$ *such that* $|s_0| = \operatorname{dist}(0, \partial\Omega) = \delta$, *it holds that*

$$H_\Omega(s_0) - \frac{\nabla f^\sigma \cdot n}{2(1 + f^\sigma)}(s_0) < 0$$

where $n(s_0)$ *is the inner unit normal to* $\partial\Omega$ *at* s_0.

Remark 2.3. This result implies that, for a time-dependent set $\Omega(t)$ evolving by the forced mean curvature motion (2.2) and such that 0 is in the interior of Ω, the forcing term f^σ acts as a repulsive source in a ring around 0. These observations can be extended to the case where the obstacle Σ is a general C^2 set.

Remark 2.4. One of the advantages of using the forced flow (2.2) with the above definition of f^σ is that, when the interface is far from the obstacle, the flow behaves almost exactly like a mean curvature flow. As the interface begins to approach the obstacle, the perturbation term forces it to maintain a minimum distance from the obstacle. It is natural to extend this idea to dynamic obstacles, and even to obstacles provided by the interface itself, typically its skeleton. This is the purpose of the next section.

Proof of Lemma 2.2. We have that $\nabla f^\sigma(s_0) \cdot n(s_0) = \partial_{n(s_0)} f^\sigma$ with $n(s_0) = -\frac{s_0}{|s_0|} = -\frac{s_0}{\delta}$. Therefore,

$$f(s_0) = \frac{1}{\sigma^N} e^{-\frac{\delta^2}{\sigma^2}} \quad \text{and} \quad \nabla f^\sigma(s_0) \cdot n(s_0) = \frac{2\delta}{\sigma^{N+2}} e^{-\frac{\delta^2}{\sigma^2}}.$$

Thanks to Lemma 2.1, it follows that

$$H_\Omega(s_0) - \frac{\nabla f^\sigma \cdot n}{2(1 + f^\sigma)}(s_0) \leq \frac{N-1}{\delta} - \frac{\frac{\delta}{\sigma^{(N+2)}} e^{-\frac{\delta^2}{\sigma^2}}}{1 + \frac{1}{\sigma^N} e^{-\frac{\delta^2}{\sigma^2}}}.$$

In order to have the left-hand term negative, it is sufficient to find an interval I_σ depending on σ such that, for all $\delta \in I_\sigma$,

$$w_\sigma(\delta) := \frac{\frac{\delta^2}{\sigma^{(N+2)}} e^{-\frac{\delta^2}{\sigma^2}}}{1 + \frac{1}{\sigma^N} e^{-\frac{\delta^2}{\sigma^2}}} > N - 1.$$

Observe that, since $0 < \sigma < 1$,

$$\max_{[0,+\infty[} w_\sigma \geq w_\sigma(\sigma\sqrt{-\ln \sigma^N}) = \frac{-\ln \sigma^N}{2}.$$

For all $0 < \sigma < \exp \frac{2(1-N)}{N}$, w_σ is continuous on $[0, +\infty)$; hence, there exists an interval I_σ containing $\sigma\sqrt{-\ln \sigma^N}$ such that, for every $\delta \in I_\sigma$, $w_\sigma(\delta) > N - 1$, and the lemma ensues. ∎

2.3.2. Case of a general fixed obstacle. Thanks to Lemma 2.1, we show in the following that, for $\sigma > 0$ small enough, we can avoid the interface colliding with a given *static obstacle*:

Theorem 2.5. *Let $\Sigma \subset \mathbb{R}^N$ be a closed k-rectifiable set and, for $0 < \sigma < 1$, let $f^\sigma dx = h^\sigma * \mathcal{H}^k \llcorner \Sigma$ where*

$$h^\sigma(x) = \frac{1}{\sigma^N} e^{-\frac{|x|^2}{\sigma^2}}.$$

Let $t \in [0, T] \mapsto \Omega(t)$ be the smooth mean curvature flow of a smooth open, bounded set. There exists $0 < \sigma < 1$ such that, if $\Sigma \subset \Omega(0)^-$ (the interior of $\Omega(0)$) and $\operatorname{dist}(\partial\Omega(0), \Sigma) \geq \delta > 0$, then for every $t \in [0, T]$, $\operatorname{dist}(\partial\Omega(t), \Sigma) \geq \delta$.

Proof. Let $t > 0$ be such that $\operatorname{dist}(\partial\Omega(t), \Sigma) = \delta$. Thanks to Lemma 2.1 and the definition of the forced mean curvature flow (2.2), for every $s_t \in \partial\Omega(t)$ satisfying $\operatorname{dist}(\partial\Omega(t), \Sigma) = \operatorname{dist}(s_t, \Sigma) = \delta$, we have that

$$V_n(s_t) = H_{\Omega(t)}(s_t) - \frac{\nabla f^\sigma(s_t) \cdot n(s_t)}{2(1 + f^\sigma(s_t))} \leq \frac{N-1}{\delta} - \frac{\nabla f^\sigma(s_t) \cdot n(s_t)}{2(1 + f^\sigma(s_t))},$$

Assume that $\Sigma \subset \Omega(t)^-$. Then

$$\lim_{\sigma \to 0} \frac{\nabla f^\sigma(s_t) \cdot n(s_t)}{f^\sigma(s_t)} = +\infty;$$

therefore, for $\sigma_t > 0$ small enough, we get that

$$V_n(s_t) \leq \frac{N-1}{\delta} - \frac{\nabla f^{\sigma_t}(s_t) \cdot n(s_t)}{2(1 + f^{\sigma_t}(s_t))} < 0.$$

By contradiction, assume now that $\Sigma \cap (\Omega(t)^-)^c$ is not empty. By the regularity theory, the flow is continuous in space so there exists an earlier time $0 \leq t' < t$ such that $\Sigma \subset \Omega(t')^-$ and $\operatorname{dist}(\partial\Omega(t'), \Sigma) = \operatorname{dist}(s', \Sigma) = \delta$ with $s' \in \partial\Omega(t')$. By the above argument, $V_n(s') < 0$ for a suitable $\sigma_{t'}$ so the distance with Σ cannot decrease, which contradicts the original assumption. It follows that, for every $t \in [0, T]$ there exists $\sigma_t > 0$ and a closest point s_t of $\partial\Omega(t)$ to Σ such that $V_n(s_t) < 0$. Using the smoothness of $\frac{\nabla f^{\sigma_t}(s) \cdot n(s)}{2(1+f^{\sigma_t}(s))}$ on a suitable open set containing Σ and strictly contained in $\Omega(t)^-$ for all t, we deduce the existence of $\sigma > 0$ such that $V_n(s_t) < 0$ for every $t \in [0, T]$. Hence, the distance between $\partial\Omega$ and Σ is bounded below by δ, which completes the proof. ∎

3. The skeleton and its approximation

There is a rich literature on *medial axes*, *skeletons*, and *cut locus* of sets with various definitions. Since it is more suitable for what we need later, we define the skeleton as follows:

Definition 3.1. The *skeleton* of a non-empty set $\Omega \subset \mathbb{R}^N$ is the singular set S_Ω of the signed distance function $\mathrm{dist}(\cdot, \Omega)$ from Ω, that is,

$$\mathrm{S}_\Omega = \{x \in \mathbb{R}^N,\ \mathrm{dist}(\cdot, \Omega) \text{ is not differentiable at } x\}.$$

Remark 3.2. Obviously, $\nabla\mathrm{dist}(\cdot, \Omega)$ is well defined on $\mathbb{R}^N \setminus \mathrm{S}_\Omega$ and takes values in $\mathbb{S}^{N-1}$. In addition (see [3]), $x \in \mathrm{S}_\Omega \setminus \partial\Omega$ if and only if there exist two distinct points $y_1, y_2 \in \partial\Omega$ such that $|x - y_1| = |x - y_2|$.

The following regularity properties are proved in [47] for the singular set of the distance function from a closed, non-empty set. They naturally extend to the signed distance function $\mathrm{dist}(\cdot, \Omega)$ from a general set $\Omega \subset \mathbb{R}^N$ with non-empty boundary.

Proposition 3.3. *If $\Omega \subset \mathbb{R}^N$ has non-empty boundary, then*

- $\mathrm{S}_\Omega \setminus \partial\Omega$ *is C^2-$(N-1)$-rectifiable.*
- *If, in addition, $\partial\Omega$ is of class C^r with $r \geq 3$, then the closure $\overline{\mathrm{S}_\Omega}$ of S_Ω is C^{r-2}-$(N-1)$-rectifiable. In particular,*
  - *the Hausdorff dimension of $\overline{\mathrm{S}_\Omega}$ is at most $(N-1)$.*
  - *the vector field $\nabla\mathrm{dist}(\cdot, \Omega)$ belongs to the space $\mathrm{SBV}_{\mathrm{loc}}(\mathbb{R}^N)$.*

Remark 3.4. Given a general set $\Omega \subset \mathbb{R}^N$ with non-empty boundary, $\overline{\mathrm{S}_\Omega}$ is not $(N-1)$-rectifiable in general. There is an example in [47] of a convex open set in $\mathbb{R}^2$ with $C^{1,1}$ boundary such that the closure of its skeleton has positive Lebesgue measure.

The boundary of Ω is the set of points where $\mathrm{dist}(\cdot, \Omega)$ vanishes. Is there a similar way to link the skeleton of Ω with the (complement of the) support of a map defined either with $\mathrm{dist}(\cdot, \Omega)$ or $\nabla\mathrm{dist}(\cdot, \Omega)$? There is no easy way to do it directly, but the skeleton can be obtained as (a subset of) the support of the distributional limit of a sequence of well-defined approximate maps.

There are however essentially two difficulties with the skeleton:

- A smooth shape may have a non-smooth, and possibly very non-smooth skeleton [47].
- There is no continuous dependence of the skeleton of a set Ω with respect to perturbations of Ω. A disk in $\mathbb{R}^2$ has its center as skeleton but it is easy to design arbitrarily small perturbations of the disk's boundary to get a collection of skeletons with Hausdorff dimension 1 and whose Hausdorff distance to the disk's center is bounded from below by a positive number.

We shall see however that using a regularized skeleton-based term yields an interesting and effective model for the numerical approximation of the mean curvature flow of thin structures.

The purpose of the next section is to provide a constructive formula for approximating a weighted Hausdorff measure supported on the skeleton $\Sigma = \mathrm{S}_\Omega$ of a non-empty set Ω.

3.1. Skeleton approximation using a constructive formula

The vector field $n = \nabla \mathrm{dist}(\cdot, \Omega)$ satisfies the equality $|n|^2 = 1$ at every point where is it defined. In particular, if n is regular at x, then

$$Sn(x) := \langle \nabla n^T(x) n(x), n(x) \rangle = 0,$$

where ∇n^T is the transpose of the matrix ∇n. This motivates the following definition:

Definition 3.5. Let $n \in SBV(\mathbb{R}^N, \mathbb{R}^N)$. The *skeletal term* of n is defined as

$$Sn := \langle n, (\nabla n)^T n \rangle.$$

Remark 3.6. For every $u \in SBV(\mathbb{R}^N)$, Du is a Radon measure that can be written (see [4]) as the sum of an absolutely continuous part and a singular part with respect to the Lebesgue measure, that is,

$$Du = D^A u + D^J u,$$

where $D^A u = \nabla^A u \mathcal{L}^N$ and $D^J u = [u] \nu \mathcal{H}^{N-1} \llcorner \Sigma$, with Σ the jump set of u, ν a unit normal on Σ, and $[u]$ the jump of u on Σ. Recall also that u is approximately differentiable almost everywhere and its approximate differential coincides with $\nabla^A u$ almost everywhere in Ω.

The skeletal term associated with $n = \nabla \mathrm{dist}(\cdot, \Omega)$ is not defined on $\Sigma := S_\Omega$, so we rather consider the skeletal term associated with a smooth approximation $n^\sigma = n * h^\sigma$ of n. Given a field $n \in SBV(\mathbb{R}^N, \mathbb{S}^{N-1})$ with smooth, $(N-1)$-dimensional jump set Σ, the next result shows a connection between the asymptotic limit of Sn^σ and Σ.

Theorem 3.7. *Let $n \in SBV(\mathbb{R}^N, \mathbb{S}^{N-1})$ with C^1-jump set Σ oriented $\mathcal{H}^{N-1}$-almost everywhere by the unit vector ν. Let $h \in C_c^\infty(\mathbb{R}^N, \mathbb{R}^+)$ be such that $\int_{\mathbb{R}^N} h\,dx = 1$, and let $h^\sigma = \frac{1}{\sigma^N} h(\frac{\cdot}{\sigma})$. Define $n^\sigma = n * h^\sigma$ and consider $Sn^\sigma = \langle n^\sigma, (\nabla n^\sigma)^T n^\sigma \rangle$. Then*

$$Sn^\sigma \to \frac{1}{12} |[n]|^2 \langle [n], \nu \rangle \, \mathcal{H}^{N-1} \llcorner \Sigma \quad \text{in } \mathcal{D}'(\mathbb{R}^N) \quad \text{as } \sigma \to 0, \tag{3.1}$$

where $[n] := n^+ - n^-$ with n^+, n^- the approximate limits of n with respect to ν on Σ, that is,

$$n^\pm(x) := \lim_{r \to 0} \fint_{B^\pm(x,r)} n(y)\, dy$$

with $B^+(x,r) = \{y \in \mathbb{R}^N \mid \langle y, \nu(x) \rangle > 0\}$ and $B^-(x,r) = \{y \in \mathbb{R}^N \mid \langle y, \nu(x) \rangle < 0\}$.

Proof. Since $n^\sigma = h^\sigma * n$, we have that

$$\partial_j n_i^\sigma = h^\sigma * \partial_j n_i = h^\sigma * \partial_j^A n_i + h^\sigma * \partial_j^J n_i = h^\sigma * \partial_j^A n_i + h^\sigma * [n_i]\nu_j\, \mathcal{H}^{N-1} \llcorner \Sigma.$$

Therefore, for every function with compact support $\varphi \in C_c^\infty(\mathbb{R}^N)$, we can write that

$$\sum_{i,j} \int_{\mathbb{R}^N} n_i^\sigma \partial_j n_i^\sigma n_j^\sigma \varphi dx = I_1^\sigma + I_2^\sigma,$$

where

$$I_1^\sigma = \sum_{i,j} \int_{\mathbb{R}^N} n_i^\sigma (h^\sigma * \partial_j^A n_i) n_j^\sigma \varphi\, dx \quad \text{and} \quad I_2^\sigma = \sum_{i,j} \int_{\mathbb{R}^N} n_i^\sigma g_{ij}^\sigma n_j^\sigma \varphi\, dx \tag{3.2}$$

with

$$g_{ij}^\sigma = h^\sigma * [n_i]\nu_j\, \mathcal{H}^{N-1} \llcorner \Sigma.$$

Without loss of generality, we can consider the restriction of these integrals to the set $Q = \Sigma(1) := \{x \in \Omega \mid d(x, \Sigma) \leq 1\}$ and assume that the map

$$\begin{aligned} \tau : \Sigma(1) &\to [-1, 1] \times \Sigma, \\ x &\mapsto (r, s) \end{aligned}$$

is a diffeomorphism, with $s = \pi_\Sigma(x)$ the normal projection of x on Σ and $r = \langle x - s, \nu(s)\rangle$, so that $x = s + r\nu(s)$. Thanks to the fact that

$$n_i^\sigma = h^\sigma * n_i \to n_i \quad \text{a.e.}, \qquad h^\sigma * \partial_j^A n_i \to \partial_j^A n_i \quad \text{a.e. as } \sigma \to 0,$$

and $|n|^2 = \sum_i n_i^2 = 1$, we get that for every $\sigma > 0$, $|n_i^\sigma (h^\sigma * \partial_j^A n_i)| \leq C|\partial_j^A n_i|$ for some $C > 0$, and

$$\sum_i n_i^\sigma (h^\sigma * \partial_j^A n_i) \to \sum_i n_i \partial_j^A n_i = \frac{1}{2}\partial_j(|n|^2) = 0 \quad \text{a.e. as } \sigma \to 0,$$

which, thanks to Lebesgue's theorem, leads to

$$\lim_{\sigma \to 0} I_1^\sigma = \sum_{i,j} \int_Q n_i \partial_j^A n_i n_j \varphi\, dx = 0.$$

In order to estimate I_2^σ defined in (3.2), by identifying $x = (r, s)_\tau$ and taking $z = r/\sigma$, we write that

$$I_2^\sigma = \sum_{i,j} \int_{-1}^1 \int_\Sigma n_i^\sigma(r,s) g_{ij}^\sigma(r,s) n_j^\sigma(r,s) \varphi(r,s) J_\Sigma(r,s) ds dr$$

$$= \sum_{i,j} \int_{-\infty}^{\infty} \int_{\Sigma} n_i^{\sigma}(\sigma z, s) g_{ij}^{\sigma}(\sigma z, s) n_j^{\sigma}(\sigma z, s) \varphi(\sigma z, s) \chi_{[-1/\sigma, 1/\sigma]}(z) \sigma \\ J_{\Sigma}(\sigma z, s) ds dz, \tag{3.3}$$

where $J_{\Sigma}(r, s) = |\det(\partial_{(r,s)} \tau^{-1}(r, s))|$ is the Jacobian of τ^{-1} at (r, s) and $\chi_{[-1/\sigma, 1/\sigma]}$ is the characteristic function of $[-1/\sigma, 1/\sigma]$.

We now study the pointwise limit of the integrand as σ goes to 0. At $(\sigma z_0, s_0) \in [-1, 1] \times \Sigma$, we have that

$$\sigma g_{ij}^{\sigma}(\sigma z_0, s_0) = \int_{\Sigma} \sigma h^{\sigma}((\sigma z_0, s_0) - (0, s))[n_i](s) \nu_j(s) ds. \tag{3.4}$$

As Σ is C^1, we can parametrize Σ locally as a graph around s_0. More precisely, up to rotation, we can assume that $\nu(s_0) = (0_{\mathbb{R}^{N-1}}, 1)$ and then there exists a neighborhood $V(s_0)$ of s_0 and $\delta > 0$ such that for all $s \in V(s_0)$, we can write that

$$s = s(u) = s_0 + (u, \Psi(u)),$$

where $u \in B^{N-1}(0, \delta)$ and $\Psi : B^{N-1}(0, \delta) \to \mathbb{R}$ is a C^1-map such that $\Psi(0) = |\nabla \Psi(0)| = 0$. For $\sigma > 0$ small enough, (3.4) can thus be written as

$$\begin{aligned} &\sigma g_{ij}^{\sigma}(\sigma z_0, s_0) \\ &\quad = \int_{B^{N-1}(0,\delta)} \sigma h^{\sigma}((\sigma z_0, s_0) - (0, s(u)))[n_i] \nu_j(s(u)) \sqrt{1 + |\nabla \Psi(u)|^2}\, du + o(1) \\ &\quad = \int_{B^{N-1}(0,\delta/\sigma)} h\Big(\frac{(\sigma z_0, s_0) - (0, s(\sigma u))}{\sigma}\Big)[n_i] \nu_j(s(\sigma u)) \sqrt{1 + |\nabla \Psi(\sigma u)|^2}\, du \\ &\qquad + o(1), \end{aligned} \tag{3.5}$$

where the second equality is obtained by replacing u with σu. Moreover, we have that

$$\begin{aligned} \frac{(\sigma z_0, s_0) - (0, s(\sigma u))}{\sigma} &= \frac{s_0 + (0_{\mathbb{R}^{N-1}}, \sigma z_0) - s_0 - (\sigma u, \Psi(\sigma u))}{\sigma} \\ &= \Big(-u, z_0 - \frac{\Psi(\sigma u)}{\sigma}\Big) \to (-u, z_0) \text{ as } \sigma \to 0. \end{aligned} \tag{3.6}$$

Together with (3.5) and (3.6), we get that

$$\sigma g_{ij}^{\sigma}(\sigma z_0, s_0) \to g(z_0)[n_i](s_0) \nu_j(s_0) \text{ as } \sigma \to 0, \tag{3.7}$$

where $g(z_0) = \int_{\mathbb{R}^{N-1}} h(-u, z_0) du = \int_{\mathbb{R}^{N-1}} h(u, z_0)\, du$.

By analogy, for σ small enough, we also have

$$n_i^{\sigma}(\sigma z_0, s_0) = \int_{-1/\sigma}^{1/\sigma} \int_{\Sigma} h^{\sigma}((\sigma z_0, s_0) - (\sigma z, s)) n_i(\sigma z, s) \sigma J_{\Sigma}(\sigma z, s)\, ds\, dz$$

$$= \int_{-1/\sigma}^{1/\sigma} \int_{B^{N-1}(0,\delta/\sigma)} h\Big(\frac{(\sigma z_0, s_0) - (\sigma z, s(\sigma u))}{\sigma}\Big)$$

$$n_i((\sigma z, s(\sigma u))) J_\Sigma(\sigma z, s(\sigma u)) \sqrt{1 + |\nabla\Psi(\sigma u)|^2}\, du\, dz. \quad (3.8)$$

Moreover, as $\sigma \to 0$,

$$\begin{aligned} n_i((\sigma z, s(\sigma u))) &\to \begin{cases} n_i^+(s_0) \text{ if } z > 0, \\ n_i^-(s_0) \text{ if } z < 0, \end{cases} \\ J_\Sigma((\sigma z, s(\sigma u))) &\to 1, \\ \frac{(\sigma z_0, s_0) - (\sigma z, s(\sigma u))}{\sigma} &\to (-u, z_0 - z). \end{aligned} \quad (3.9)$$

Notice that the second limit is due to the fact that $J_\Sigma(r,s) = 1 + H_\Sigma(s)r + o(r)$; see [57].

Thanks to (3.8) and (3.9), we get that

$$\begin{aligned} n_i(\sigma z_0, s_0) \to &\int_0^{+\infty}\int_{\mathbb{R}^{N-1}} h(-u, z_0 - z) n_i^+(s_0)\, du\, dz \\ &+ \int_{-\infty}^0 \int_{\mathbb{R}^{N-1}} h(-u, z_0 - z) n_i^-(s_0)\, du\, dz \\ &= \Big(\int_{-\infty}^{z_0} g(z)\, dz\Big) n_i^+(s_0) + \Big(\int_{z_0}^{+\infty} g(z)\, dz\Big) n_i^-(s_0) \\ &= G(z_0) n_i^+(s_0) + \Big(1 - G(z_0)\Big) n_i^-(s_0), \end{aligned} \quad (3.10)$$

as $\sigma \to 0$, where $G(z_0) = \int_{-\infty}^{z_0} g(z) dz$.

Lastly, together with (3.3), (3.7), (3.9), and (3.10), we obtain that

$$\begin{aligned} \lim_{\sigma\to 0} I_2^\sigma &= \sum_{i,j} \int_\Sigma \int_{\mathbb{R}} \big(G(z) n_i^+(s) + (1 - G(z)) n_i^-(s)\big)(g(z)[n_i]\nu_j) \\ &\qquad \cdot \big(G(z) n_j^+(s) + (1 - G(z)) n_j^-(s)\big)\, dz\, \varphi(0, s)\, ds \\ &= \sum_i \int_\Sigma \int_{\mathbb{R}} G(z) g(z)[n_i](G(z) n_i^+ + (1 - G(z)) n_i^-)\langle n^+, \nu\rangle(s)\varphi(0, s)\, ds \\ &\quad + \sum_i \int_\Sigma \int_{\mathbb{R}} (1 - G(z)) g(z)[n_i](G(z) n_i^+ \\ &\qquad + (1 - G(z)) n_i^-)\langle n^-, \nu\rangle(s)\varphi(0, s)\, ds, \end{aligned}$$

which, thanks to the fact that $\sum_i (1 - n_i^+ n_i^-) = \frac{|[n]|^2}{2}$, leads to

$$\begin{aligned} \lim_{\sigma\to 0} I_2^\sigma &= \sum_i \int_\Sigma \int_{\mathbb{R}} G(z) g(z)(2G(z) - 1)(1 - n_i^+ n_i^i)\langle n^+, \nu\rangle(s)\varphi(0, s)\, ds \\ &\quad + \sum_i \int_\Sigma \int_{\mathbb{R}} (1 - G(z)) g(z)(2G(z) - 1)(1 - n_i^+ n_i^i)\langle n^-, \nu\rangle(s)\varphi(0, s)\, ds \end{aligned}$$

$$
\begin{aligned}
&= \int_\Sigma \Big(\int_\mathbb{R} G(z) g(z)(2G(z)-1)\, dz \Big) \frac{|[n]|^2}{2} \langle n^+, \nu\rangle(s)\varphi(0,s)\, ds \\
&\quad + \int_\Sigma \Big(\int_\mathbb{R} (1-G(z)) g(z)(2G(z)-1)\, dz \Big) \frac{|[n]|^2}{2} \langle n^-, \nu\rangle(s)\varphi(0,s)\, ds \\
&= \frac{1}{12} \int_\Sigma |[n]|^2 \langle [n], \nu\rangle \varphi(0,s)\, ds = \Big\langle \frac{1}{12} |[n]|^2 \langle [n], \nu\rangle\, \mathcal{H}^{N-1} \llcorner \Sigma, \varphi \Big\rangle,
\end{aligned}
$$

and Theorem 3.7 ensues. ∎

3.2. Numerical illustrations

We provide in this section numerical illustrations of Theorem 3.7 for various sets in $\mathbb{R}^2$ and $\mathbb{R}^3$. More precisely, we compute, for each set Ω, numerical approximations on a Cartesian grid of $n = \nabla \operatorname{dist}(\cdot, \Omega)$, of $n^\sigma = h^\sigma * n$ with

$$
h^\sigma = \frac{1}{\sigma^N} e^{-\pi \frac{|x|^2}{\sigma^2}}
$$

a Gaussian kernel, and of the approximate skeletal term Sn^σ.

3.2.1. 2D examples. Figure 2 shows, for three 2D sets whose boundaries consist of, respectively,

- two concentric circles,
- two parallel lines,
- a rectangle,

the values taken by the approximate skeletal term Sn^σ for different choices of the regularization parameter $\sigma > 0$.The resolution is set to 2^7 nodes for each grid dimension. On each numerical example, Sn^σ charges essentially the (codimension 1) main part of the skeleton Σ, with a weight that depends on the normal ν of Σ, which is consistent with the term $\langle [n], \nu\rangle$ in (3.1). Negligible parts of the skeleton (i.e., of codimension greater than 1) are also detected; for example, the center of the ring is activated in the first example.

3.2.2. 3D examples. We perform a similar test in 3D with a numerical resolution of 2^7 nodes for each grid dimension. The examples used for the illustration in Figure 3 have as boundaries, respectively,

- two concentric spheres,
- two parallel planes,
- a circular torus.

The values taken by the skeletal term Sn^σ are captured on the three hyperplanes $\{x_1 = 0\}$, $\{x_2 = 0\}$, and $\{x_3 = 0\}$, respectively. As for the 2D examples, the skeletons are correctly localized by Sn^σ.

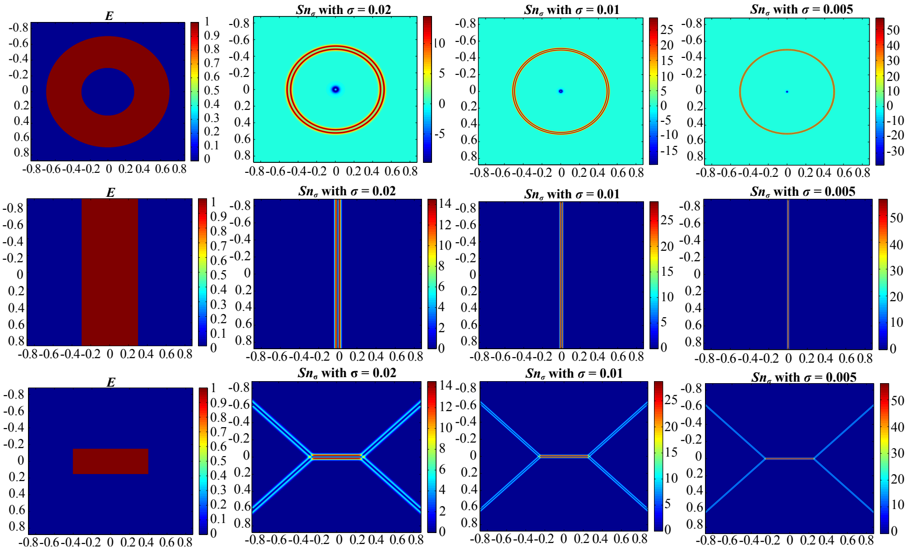

Figure 2. Numerical values of the approximate skeletal term Sn^σ for various $2D$ configurations, and for various values of σ. The first figure of each line corresponds to the considered set. Columns 2, 3, and 4 show the values of the scalar field Sn^σ for, respectively, $\sigma = 0.02$, 0.01, and 0.005.

3.3. Skeleton and asymptotic expansion of the skeletal term

According to Theorem 3.7, the skeletal term Sn^σ approximates the codimension 1 jump set of n weighted by the height of the jump and the angle with the normal to the set. At order 0, Sn^σ does not charge at the limit higher codimensional singular parts of the skeleton. To identify these parts, we believe it is necessary to look at higher order terms in the expansion of Sn^σ with respect to σ, which yields the conjecture below. Although we were not able to prove it in full generality, we will illustrate it with two examples, a round sphere in $\mathbb{R}^N$ and a circular torus in $\mathbb{R}^3$.

Conjecture 3.8. *Let $\Omega \subset \mathbb{R}^N$ be a non-empty open set, $n = \nabla \mathrm{dist}(\cdot, \Omega)$, and $n^\sigma = n * h^\sigma$, with $h^\sigma = \frac{1}{\sigma^N} h(\frac{\cdot}{\sigma})$ where $h \in C_c^\infty(\mathbb{R}^N, \mathbb{R}^+)$ is such that $\int_{\mathbb{R}^N} h dx = 1$. Let $Sn^\sigma = \langle n^\sigma, (\nabla n^\sigma)^T n^\sigma \rangle$. Then*

$$Sn^\sigma \sim \sum_{k=0}^{N-1} \sigma^k \alpha_k \mathcal{H}^{N-1-k} \llcorner \Sigma_k, \tag{3.11}$$

where

- *α_k are $\mathbb{R}$-valued density functions,*

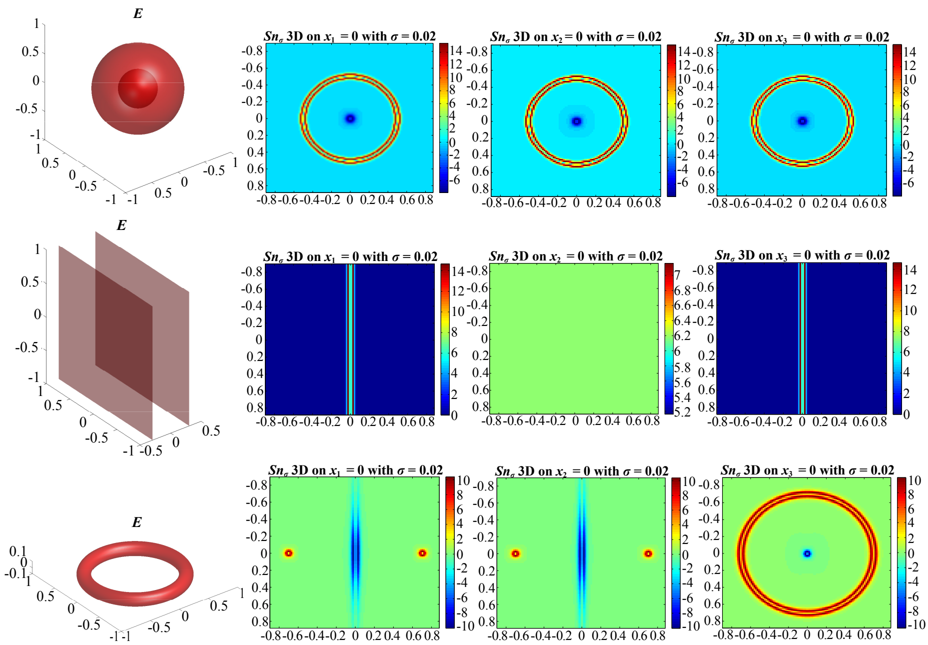

Figure 3. Numerical values of the skeletal term Sn^σ for $3D$ examples. Each line shows the considered set, then the values taken by the skeletal term on the planes $\{x_1 = 0\}$, $\{x_2 = 0\}$, and $\{x_3 = 0\}$, respectively.

- *Σ_k are $(N-1-k)$-dimensional sets,*
- *the skeleton $\Sigma = S_\Omega$ of Ω satisfies $\Sigma = \bigcup_k \Sigma_k$.*

3.3.1. Expansion of the skeletal term of a sphere in $\mathbb{R}^N$. The skeleton Σ of the signed distance function n to the sphere is a point. Without loss of generality, we assume that $\Sigma = \{0_{\mathbb{R}^N}\}$ and

$$n(x) = -\frac{x}{|x|}, \quad \forall x \neq 0.$$

Thanks to the definition of n^σ and its symmetric properties, we get that

$$n^\sigma(x) = w\Big(\frac{|x|}{\sigma}\Big) n(x), \quad \forall x \neq 0, \tag{3.12}$$

where $w : \mathbb{R}^+ \to [0,1]$ is a smooth function such that $w(0) = 0$ and $\lim_{t\to+\infty} w(t) = 1$. Since $\sum_{i,j} n_i \partial_j n_i n_j = 0$ almost everywhere, we get from (3.12) that

$$
\begin{aligned}
Sn^\sigma(x) &= \sum_{i,j} w\Big(\frac{|x|}{\sigma}\Big) n_i \Big(w\Big(\frac{|x|}{\sigma}\Big)\partial_j n_j\Big) w\Big(\frac{|x|}{\sigma}\Big) n_j \\
&= -\sum_j \Big(w\Big(\frac{|x|}{\sigma}\Big)\Big)^2 w'\Big(\frac{|x|}{\sigma}\Big) n_j \frac{x_j}{\sigma|x|} \\
&= -\frac{1}{\sigma}\Big(w\Big(\frac{|x|}{\sigma}\Big)\Big)^2 w'\Big(\frac{|x|}{\sigma}\Big).
\end{aligned}
$$

Therefore, for every $\varphi \in C_c^\infty(\mathbb{R}^N)$, we have that

$$
\begin{aligned}
\langle Sn^\sigma, \varphi\rangle &= -\frac{1}{\sigma}\int_{\mathbb{R}^N} \Big(w\Big(\frac{|x|}{\sigma}\Big)\Big)^2 w'\Big(\frac{|x|}{\sigma}\Big)\varphi(x)\,dx \\
&= -\frac{1}{\sigma}\int_0^\infty \int_{\mathbb{S}_r} \Big(w\Big(\frac{r}{\sigma}\Big)\Big)^2 w'\Big(\frac{r}{\sigma}\Big)\varphi(r,s) ds_{\mathbb{S}_r} dr \\
&= -\frac{1}{\sigma}\int_0^\infty \Big(w\Big(\frac{r}{\sigma}\Big)\Big)^2 w'\Big(\frac{r}{\sigma}\Big) r^{N-1}\Big(\int_{\mathbb{S}^{N-1}} \varphi(r,s)\,ds\Big)\,dr \\
&= -\sigma^{N-1}\int_0^\infty w(u)^2 w'(u)\Big(\int_{\mathbb{S}^{N-1}} \varphi(\sigma u, s)\,ds\Big) u^{N-1}\,du \\
&\sim -\sigma^{N-1}\varphi(0)\int_{\mathbb{R}^N} w(|x|)^2 w'(|x|) dx,
\end{aligned}
$$

which gives

$$
\frac{1}{\sigma^{N-1}}\langle Sn^\sigma, \varphi\rangle \to \Big(-\int_{\mathbb{R}^N} w(|x|)^2 w'(|x|) dx\Big)\varphi(0),
$$

as $\sigma \to 0$.

3.3.2. Expansion for a circular torus in $\mathbb{R}^3$. We now consider a circular torus $\Omega_\sigma = \{x \in \mathbb{R}^3,\ d(x,\Sigma) \le \sigma\}$ whose skeleton $\Sigma = \{(x_1, x_2, 0) \in \mathbb{R}^3,\ x_1^2 + x_2^2 = 2^2\}$ is a planar circle in $\mathbb{R}^3$. The same kind of argument as below can be actually used for any regular closed curve in $\mathbb{R}^3$. For $\sigma > 0$ small enough, and for every $x \in \Omega_\sigma$, we write that

$$
x = s + \sigma u,
$$

where $s = \pi_\Sigma(x)$ is the orthogonal projection of x on Σ and $u \in N_s\Sigma$ is a unit vector of the normal space at s. In particular, the map

$$
\begin{aligned}
\tau_\sigma : N &\to \Omega_\sigma \\
(s,u) &\mapsto s + \sigma u,
\end{aligned}
$$

where $N = \bigcup_{s\in\Sigma}\{s\} \times N_s := \bigcup_{s\in\Sigma}\{s\} \times \{u \in N_s\Sigma,\ |u| = 1\}$, is a diffeomorphism. We take the canonical orthonormal basis on Ω_σ denoted by (e_s, e_{u_1}, e_{u_2}). Thanks to the definition of τ_σ, for every $x_0^\sigma \in \Omega_\sigma$, we can write that

$$
x_0^\sigma = \tau_\sigma(s_0, u_0).
$$

Using integration by substitution, we obtain that

$$\begin{aligned} n^\sigma(x_0^\sigma) &= \int_{\Omega_\sigma} n(y) h^\sigma(x_0^\sigma - y)\, dy \\ &= \int_\Sigma \Big(\int_{N_s} n(\tau_\sigma(s,u)) h^\sigma(\tau_\sigma(s_0,u_0) - \tau_\sigma(s,u)) J_{\tau_\sigma}(s,u)\, du \Big)\, ds \\ &= \frac{1}{\sigma^3} \int_\Sigma \Big(\int_{N_s} n(\tau_\sigma(s,u)) h\Big(\frac{\tau_\sigma(s_0,u_0) - \tau_\sigma(s,u)}{\sigma} \Big) J_{\tau_\sigma}(s,u)\, du \Big)\, ds \\ &= \frac{1}{\sigma^3} \int_\Sigma \Big(\int_{N_s} n(\tau_\sigma(s,u)) h\Big(\frac{s_0 - s}{\sigma} + (u_0 - u) \Big) J_{\tau_\sigma}(s,u)\, du \Big)\, ds, \end{aligned} \tag{3.13}$$

where $J_{\tau_\sigma}(s,u)$ is the Jacobian of τ_σ. Since $J_{\tau_\sigma}(s,u) = \sigma^2 J_{\tau_1}(s,u) = O(\sigma^2)$, thanks to (3.13) and the symmetries of n and h, we get that

$$\partial_u n^\sigma(x_0^\sigma) = O\Big(\frac{1}{\sigma}\Big) \quad \text{and} \quad \partial_s n^\sigma(x_0^\sigma) = 0, \tag{3.14}$$

as $\sigma \to 0$. Finally, injecting (3.14) into Definition 3.5 of Sn^σ, we have that

$$\begin{aligned} \langle Sn^\sigma, \varphi \rangle &= \sum_{i,j} \int_{\Omega_\sigma} n_i^\sigma \partial_j n_i^\sigma n_j^\sigma\, \varphi\, dx \\ &= O\Big(\int_\Sigma \Big(\int_{N_s} \partial_u n^\sigma(\tau_\sigma(s,u)) \varphi(\tau_\sigma(s,u)) J_{\tau_\sigma}(s,u)\, du \Big)\, ds \Big) \\ &= O\Big(\sigma \int_\Sigma \varphi(s)\, ds \Big), \end{aligned}$$

as $\sigma \to 0$.

Remark 3.9. In the numerical computations of Figures 2 and 3, the magnitude of the skeletal term appears to be linear with respect to σ, independently of the local dimension of the skeleton, and this is not in contradiction with (3.11). Consider for instance the two concentric circles of Figure 2. The skeletal term calculated at the center has the same order of magnitude (up to a sign difference) as on the circle. This is due to the fact that δ_0 charges numerically the inverse of the pixel area, that is, $\delta_0(\Sigma) \simeq \frac{1}{\sigma^2}$. Besides, the uniform measure on the discrete circle satisfies $\mu_1(\Sigma) \simeq \frac{1}{L\sigma}$, since the circle of length L is approximated numerically by a band of area $L\sigma$ in $2D$. Therefore, $\sigma\delta_0(\Sigma) \simeq L\mu_1(\Sigma) \simeq \frac{1}{\sigma}$, which justifies the fact that the skeletal term in Figure 2 has approximately the same magnitude at the center and on the circle.

4. An Allen–Cahn equation with a skeleton-aware forcing term

What is a natural candidate phase field model to approximate the mean curvature flow of a thin structure? Thanks to the results and remarks from the previous sections, a natural approach is to consider a phase field approximation u^ε of a tubular neighborhood of the thin structure, and to use the Allen–Cahn equation coupled with a skeletal term, that is,

$$\partial_t u^\varepsilon = \Delta u^\varepsilon - \frac{W'(u^\varepsilon)}{\varepsilon^2}(1 + f^\sigma_{u^\varepsilon}) \tag{4.1}$$

where

$$f^\sigma_{u^\varepsilon} = c(h^\sigma * |Sn^\sigma_{u^\varepsilon}|) \quad \text{and} \quad n^\sigma_{u^\varepsilon} = h^\sigma * \frac{\nabla u^\varepsilon}{|\nabla u^\varepsilon|}.$$

Here, h^σ is a smooth kernel, typically a Gaussian kernel of standard deviation $\sigma > 0$, and c is a constant to be chosen sufficiently large in order to enforce the thickness constraint.

The theoretical analysis of such a phase field model seems rather difficult and is beyond the scope of this article. Our first goal is to propose a semi-implicit numerical discretization of this model and to illustrate its potential for handling a minimum thickness constraint and, more generally, for obtaining, at least formally, approximations of motion by mean curvature of filaments and other fine structures.

The code used for the numerical experiments shown below can be downloaded from a GitHub repository.[1]

Remark 4.1. In all the numerical simulations presented in this section, we do not calculate at each time step either the distance function from the interface or the skeleton of the interface, but only the forcing term $f^\sigma_{u^\varepsilon}$. This term charges implicitly the singularities of ∇u_ε, thus imposes a repulsive force related to the skeleton of the interface. It is clear that, in practice, the skeleton is not stable with respect to small perturbations of the interface. This is why we use a convolution kernel of size σ, which in a way allows greater stability by considering a regularization of the measure supported on the skeleton, rather than using the skeleton directly.

4.1. Numerical discretization of the penalized Allen–Cahn equation and a first numerical simulation

To approximate numerically the above flow, we propose a quasi-static approach with explicit integration of the skeletal term. More precisely, we consider the sequence of approximate solutions $(u^n)_n$ defined recursively by $u^{n+1}(x) \simeq v(x, \delta_t)$ where v is solution to the following PDE:

$$\begin{cases} \partial_t v(x,t) = \Delta v(x,t) - \dfrac{W'(v(x,t))}{\varepsilon^2}(1 + f^\sigma_{u^n}(x)), \\ v(\cdot, 0) = u^n \end{cases} \tag{4.2}$$

and δ_t represents the time step. Notice that this equation is variational as it is the L^2-gradient flow of the perturbed Cahn–Hilliard energy

$$J^\varepsilon_{u^n}(v) = \int_{\mathbb{R}^N} \Big(\frac{\varepsilon}{2}|\nabla v|^2 + \frac{1}{\varepsilon} W(v)(1 + f^\sigma_{u^n})\Big) dx.$$

[1] https://github.com/eliebretin/skeleton_Allen_Cahn.git visited on 30 March 2026

Equation (4.2) is solved numerically in a box Q with periodic boundary conditions. We use a semi-implicit approach based on a convex-concave splitting of the perturbed Cahn–Hilliard energy. More precisely, we define the solution u^n as an approximation of u at time $n\delta_t$ given by the scheme

$$\frac{u^{n+1}-u^n}{\delta_t} = (\Delta u^{n+1} - \frac{\alpha}{\epsilon^2}u^{n+1}) - \Big((1+f^{\sigma}_{u^n})\frac{W'(u^n)}{\varepsilon^2} - \frac{\alpha}{\epsilon^2}u^n\Big).$$

The stabilization coefficient α is assumed to be sufficiently large to ensure the concavity of the functional

$$v \mapsto \int_Q (1+f^{\sigma}_{u^n})\frac{W(v)}{\epsilon^2} - \alpha\frac{v^2}{2\varepsilon^2}dx.$$

Indeed, it suffices to choose

$$\alpha > \max_{0\le s\le 1} |1+f^{\sigma}_{u^n}|\,|W''(s)| = \max\{1, c\sigma^{-2}\}$$

to ensure that the perturbed Cahn–Hilliard energy is non-increasing over the iterations, that is,

$$J^{\varepsilon}_{u^n}(u^{n+1}) \le J^{\varepsilon}_{u^n}(u^n),$$

and the scheme is unconditionally energy-stable.

A convenient formulation of the scheme is

$$u^{n+1} = \Big[I_d - \delta_t(\Delta - \frac{\alpha}{\epsilon^2}I_d)\Big]^{-1}\Big(u^n - \delta_t\Big((1+f^{\sigma}_{u^n}(x))\frac{W'(u^n)}{\varepsilon^2} - \frac{\alpha}{\epsilon^2}u^n\Big)\Big)$$

because the operator $(I_d - \delta_t(\Delta - \frac{\alpha}{\epsilon^2}I_d))^{-1}$ can be computed very efficiently in Fourier space using the Fast Fourier Transform and periodic boundary conditions on Q.

In practice, we consider the box $Q = [-0.5, 0.5]^3$, discretized with N nodes on each axis. All 3D numerical experiments presented in this section are obtained using a resolution of $N = 2^7$, a phase-field parameter $\varepsilon = 2/N$, and $\delta_t = \varepsilon^2$. As for the skeletal term, we set $\sigma^2 = 0.1\varepsilon^2$ and $c = 0.35\varepsilon N^3$.

The first numerical experiment illustrates the influence of the skeletal term in our model. We consider a dumbbell as the initial set, and we recall that its evolution by classical phase field mean curvature flow yields a topology change in finite time. This is illustrated on the first line of Figure 4 where we plot the 0-level set of an approximate solution u^n of the Allen–Cahn equation, computed at different times $t^n = nh$, without using the skeletal term (which corresponds to setting $c = 0$). On the second line, we plot the 0-level set of the approximate solution u^n of our model. Clearly, the skeletal term enforces the topological conservation other the iterations.

4.2. Second simulation: comparison with a codimension 2 mean curvature flow

We consider the evolution of a planar circle in $3D$ as an example of a smooth codimension 2 mean curvature flow. As the circle lies in a plane, its evolution is actually 2D. More

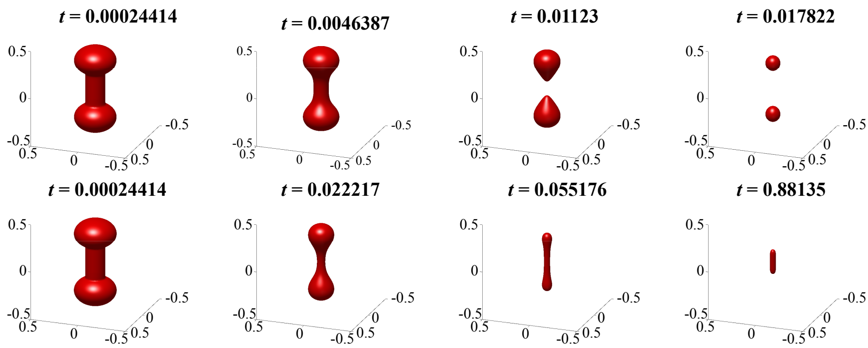

Figure 4. Evolution of a dumbbell: the solution u^n shown at different times t. The first and second lines correspond to the approximate mean curvature flow with or without, respectively, the skeletal term.

precisely, the evolving curve is a shrinking circle whose radius evolves with time as

$$R(t) = \sqrt{R(0)^2 - 2t}.$$

We show in Figure 5 the numerical approximations provided by our model at different times $t^n = nh$. They clearly show the evolution of an approximate circle whose radius decreases over the iterations. We also illustrate in the last figure that the evolution over the iterations of the squared mass $(\int_Q u^n(x)\,dx)^2$ of u^n is consistent, except at the very beginning of the simulation, with the linear decreasing of the squared circle's radius. In other words, the approximate circle evolves consistently with the higher codimension mean curvature flow up to a multiplicative factor, which is close to 8 for the parameters used in this numerical experiment. One possible reason for the initial "bad" behavior is an inconsistent initialization, which is quickly regularized by the flow.

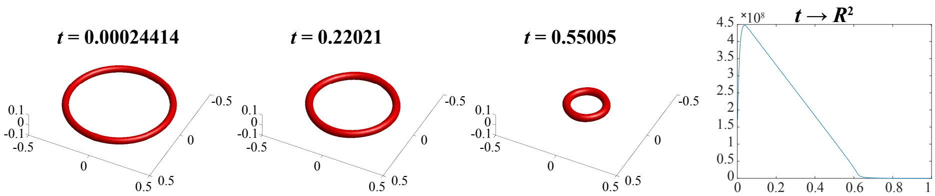

Figure 5. Evolution in 3D of a circle's tubular approximation: the approximate solution u^n is shown at different times. The squared mass $(\int_Q u^n(x)dx)^2$ over the iterations is plotted on the right figure.

To further justify the link, at least formally, between our model and a higher codimension mean curvature flow, we compare in Figure 6 the numerical evolution in 3D of a planar curve with the evolution approximated with our model of a 3D tubular approximation of the curve. The planar evolution of the curve is approximated with the 2D

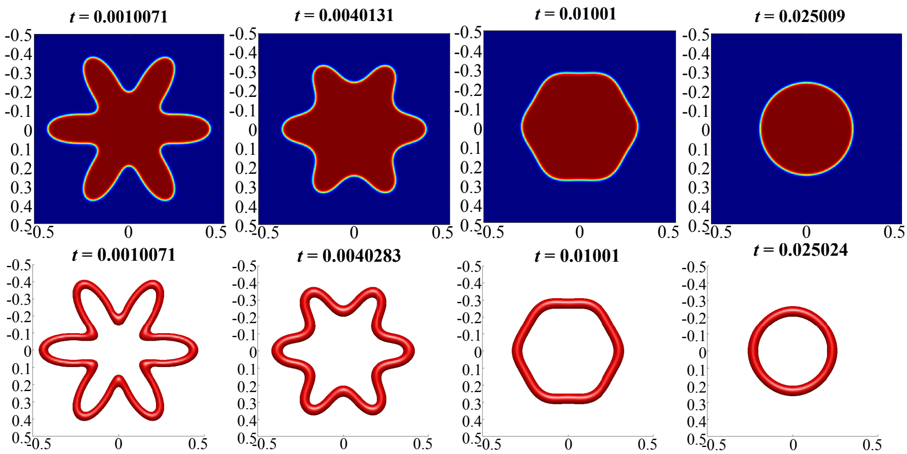

Figure 6. First line: a planar curve in 3D evolving by mean curvature approximated with the 2D Allen-Cahn equation. Second line: a 3D tubular neighborhood of the curve evolving by our 3D Allen-Cahn equation with skeletal penalty.

Allen–Cahn equation, which provides with theoretical guarantees an approximation of the real 2D mean curvature flow, as recalled in the introduction. The two dynamics look very similar.

4.3. Analytical comparison with a codimension 2 mean curvature flow

The simulations of the previous section show two configurations where the dynamics obtained with our model is consistent with a codimension 2 mean curvature flow. We develop in this section an analysis which provides an additional argument in favor of consistency: we compare the evolution by mean curvature of a closed smooth curve Γ embedded in 3D with the evolution of a small tubular neighborhood of Γ moved by the forced mean curvature flow

$$V = H + g_\sigma \tag{4.3}$$

where

$$g_\sigma = \frac{-\nabla^\perp f^\sigma}{2(1+f^\sigma)},$$

$f^\sigma dx = h^\sigma * \mathcal{H}^1 \llcorner \Gamma$, and $h^\sigma(x) = \frac{1}{\sigma^3} e^{-\frac{|x|^2}{\sigma^2}}$. We consider an arc-length parametrization $\alpha : [0, L) \mapsto \mathbb{R}^3$ of Γ, and, for each $s \in [0, L)$, we denote $T(s) = \alpha'(s)$ the tangent vector at $\alpha(s)$, and $(T(s), N(s), B(s))$ the Frenet–Serret frame, with $N(s)$ the unit normal and $B(s)$ the unit binormal [35]. We recall the Frenet–Serret formulas [35]

$$\begin{cases} T_s = kN, \\ N_s = -kT + \tau B, \\ B_s = -\tau N, \end{cases}$$

where $k(s) = |\alpha''(s)|$ is the scalar curvature of Γ at $\alpha(s)$, and $\tau(s)$ the torsion. The normal plane to Γ at $\alpha(s)$ is spanned by $(N(s), B(s))$ thus, choosing $0 < \sigma < \frac{1}{\max_{[0,L)} k(s)}$, the boundary of the σ-tubular neighborhood of Γ is the surface parametrized by

$$x : (s, \theta) \in [0, L) \times [-\pi, \pi) \mapsto \alpha(s) + \sigma n(s, \theta),$$

where $n(s, \theta) = N(s)\cos\theta + B(s)\sin\theta$. Observe that $n(s, \theta)$ is a unit outer normal to the surface at $x(s, \theta)$. Indeed, $|n|^2 = 1$, thus $\langle n, n_s\rangle = \langle n, n_\theta\rangle = 0$. In addition, $x_s = T + \sigma n_s$ and $x_\theta = \sigma n_\theta$; therefore, $\langle n, x_s\rangle = \langle n, x_\theta\rangle = 0$. Using the Frenet–Serret formulas, we calculate that

$$\begin{aligned} n_\theta &= -(\sin\theta)N + (\cos\theta)B, \\ n_s &= (\cos\theta)N_s + (\sin\theta)B_s = -k(\cos\theta)T + \tau(\cos\theta)B + (\sin\theta)B_s \\ &= -k(\cos\theta)T + \tau n_\theta + \tau(\sin\theta)N + (\sin\theta)B_s = -k(\cos\theta)T + \tau n_\theta, \\ x_s &= T + \sigma n_s = (1 - \sigma k\cos\theta)T + \sigma\tau n_\theta. \end{aligned}$$

Both T and n_θ are unit vectors and orthogonal to n so (T, n_θ) is an orthonormal basis of the tangent plane to the surface at $x(s, \theta)$. We observe that $dn = n_s ds + n_\theta d\theta$; therefore,

$$dn(T) = n_s ds(T) + n_\theta d\theta(T).$$

By the calculations above, we have that $T = \frac{1}{1-\sigma k\cos\theta}x_s - \frac{\sigma\tau}{1-\sigma k\cos\theta}n_\theta$. As $x_\theta = \sigma n_\theta$, we get that

$$T = \frac{1}{1 - \sigma k\cos\theta}x_s - \frac{\tau}{1 - \sigma k\cos\theta}x_\theta;$$

therefore,

$$ds(T) = \frac{1}{1 - \sigma k\cos\theta} \quad \text{and} \quad d\theta(T) = -\frac{\tau}{1 - \sigma k\cos\theta},$$

and finally,

$$dn(T) = \frac{1}{1 - \sigma k\cos\theta}n_s - \frac{\tau}{1 - \sigma k\cos\theta}n_\theta.$$

Besides, the above formulas for x_s and T imply that

$$x_s = (1 - \sigma k\cos\theta)T + \sigma\tau n_\theta = x_s - \tau x_\theta + \sigma\tau n_\theta; \quad \text{hence,} \quad n_\theta = \frac{1}{\sigma}x_\theta.$$

Thus,

$$dn(n_\theta) = n_s ds(n_\theta) + n_\theta d\theta(n_\theta) = \frac{n_\theta}{\sigma}.$$

It follows that

$$\begin{pmatrix} dn(T) \\ dn(n_\theta) \end{pmatrix} = \begin{pmatrix} \frac{1}{1-\sigma k\cos\theta} & -\frac{\tau}{1-\sigma k\cos\theta} \\ 0 & \frac{1}{\sigma} \end{pmatrix} \begin{pmatrix} n_s \\ n_\theta \end{pmatrix}$$
$$= \begin{pmatrix} \frac{1}{1-\sigma k\cos\theta} & -\frac{\tau}{1-\sigma k\cos\theta} \\ 0 & \frac{1}{\sigma} \end{pmatrix} \begin{pmatrix} -k\cos\theta & \tau \\ 0 & 1 \end{pmatrix} \begin{pmatrix} T \\ n_\theta \end{pmatrix},$$

thus,

$$\begin{pmatrix} dn(T) \\ dn(n_\theta) \end{pmatrix} = \begin{pmatrix} \frac{-k\cos\theta}{1-\sigma k\cos\theta} & 0 \\ 0 & \frac{1}{\sigma} \end{pmatrix} \begin{pmatrix} T \\ n_\theta \end{pmatrix},$$

which completes the identification of the Weingarten map of the surface at $x(s,\theta)$ [35]. We deduce that the mean curvature vector at $x(s,\theta)$ is

$$\begin{aligned} H(s,\theta) &= -[\langle T, dn(T)\rangle + \langle n_\theta, dn(n_\theta)\rangle]n \\ &= \Big(\frac{k\cos\theta}{1-\sigma k\cos\theta} - \frac{1}{\sigma}\Big)(N(s)\cos\theta + B(s)\sin\theta). \end{aligned}$$

The barycenter of each normal section of the σ-tubular neighborhood is a point $\alpha(s) \in \Gamma$. Let us compare the average velocity over a σ-normal circle

$$\theta \in [-\pi,\pi) \mapsto \alpha(s) + \sigma n(s,\theta)$$

moved by (4.3) with the velocity at $\alpha(s)$ of Γ moved by mean curvature. The integral of the mean curvature vector along the σ-circle reduces to

$$\begin{aligned} \int_{-\pi}^{\pi} H(s,\theta)d\theta &= \int_{-\pi}^{\pi} \frac{k\cos\theta}{1-\sigma k\cos\theta}(N(s)\cos\theta + B(s)\sin\theta)d\theta \\ &= N(s)\int_{-\pi}^{\pi}\frac{k\cos^2\theta}{1-\sigma k\cos\theta}d\theta + B(s)\int_{-\pi}^{\pi}\frac{k\cos\theta\sin\theta}{1-\sigma k\cos\theta}d\theta \\ &= N(s)\int_{-\pi}^{\pi}\frac{k\cos^2\theta}{1-\sigma k\cos\theta}d\theta. \end{aligned}$$

Recall the standard formula

$$\int_0^{\pi}\frac{\cos(nt)}{1+a\cos t}dt = \frac{\pi}{\sqrt{1-a^2}}\Big(\frac{\sqrt{1-a^2}-1}{a}\Big)^n, \quad 0 < a^2 < 1,\ n \geq 0.$$

We calculate here that

$$\begin{aligned} \int_{-\pi}^{\pi}\frac{k\cos^2\theta}{1-\sigma k\cos\theta}d\theta &= \int_0^{\pi}\frac{k\cos 2\theta}{1-\sigma k\cos\theta}d\theta + \int_0^{\pi}\frac{k}{1-\sigma k\cos\theta}d\theta \\ &= \frac{k\pi}{\sqrt{1-\sigma^2k^2}}\Big[1 + \Big(\frac{\sqrt{1-\sigma^2k^2}-1}{\sigma k}\Big)^2\Big], \end{aligned}$$

so the integrated mean curvature vector on the normal σ-circle centered at $\alpha(s)$ is

$$\int_{-\pi}^{\pi} H(s,\theta)d\theta = \frac{k\pi}{\sqrt{1-\sigma^2k^2}}\Big[1 + \Big(\frac{\sqrt{1-\sigma^2k^2}-1}{\sigma k}\Big)^2\Big]N(s);$$

therefore, the average mean curvature vector on the normal σ-circle centered at $\alpha(s)$ is

$$\bar{H}(s) = \frac{k}{2}[1 + O(\sigma^2 k^2)]N(s).$$

The velocity of the surface at $x(s,\theta)$ under flow (4.3) is

$$V_{x(s,\theta)} = H(s,\theta) + g_\sigma(s,\theta).$$

The skeletal term satisfies $g_\sigma(s,\theta) = -g_\sigma(s+\pi,\theta)$ so the average velocity on the normal σ-circle centered at $\alpha(s)$ is

$$\bar{V}_{x(s)} = \bar{H}(s) = \frac{k}{2}[1 + O(\sigma^2 k^2)]N(s),$$

which is, up to a constant multiplier, consistent with the velocity at $\alpha(s)$ of Γ moved by mean curvature. The forced mean curvature flow of the tubular σ-neighborhood of Γ is therefore consistent with the codimension 2 mean curvature flow of the curve.

4.4. Applications to smooth or non-smooth curves (and filaments) in 3D

We present two filament evolutions (i.e., smooth curves) in Figure 7. The first line shows the evolution of a simple filament which converges, using periodic boundary conditions, to a simple line. The second line shows the evolution of a more complex filament with the presence of a triple junction.

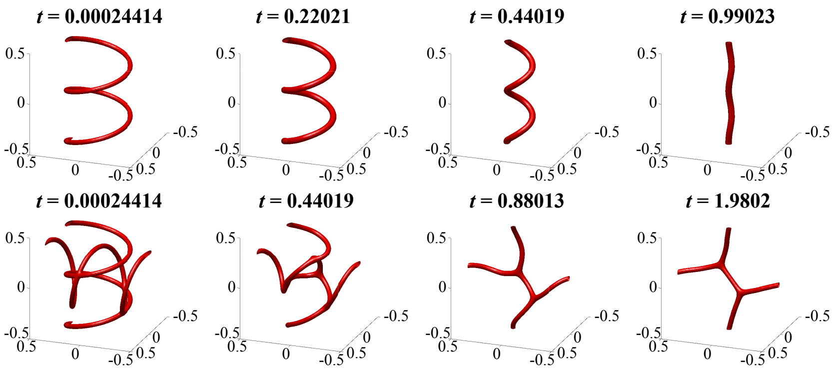

Figure 7. Numerical approximations of mean curvature flows of filaments: each line corresponds to the evolution obtained at different times from a given initial condition.

To get a better idea of the numerical flows calculated with our model, videos (in .avi format) can be downloaded from the following addresses:

- Video of the flow shown in Figure 7, top: Filament 1.[2]

[2] https://plmbox.math.cnrs.fr/f/08600d79871e45149d28/ visited on 30 March 2026

- Video of the flow shown in Figure 7, bottom: Filament 2.[3]
- In the second video, the filament remains connected but the inner cycle disappears. It is actually possible to play with that behavior by simply changing the weight of the skeletal term: a higher weight c yields a higher sensitivity. This is the choice made for the numerical simulation shown in the following third video where the inner cycle is conserved: Filament 3.[4] More precisely, the mean curvature of a linear-type σ-tubular neighborhood is approximately $\frac{1}{\sigma}$, and it is of order $\frac{2}{\sigma}$ for an inner cycle associated with a circle of radius σ. In the case of the Filament 2 video, the value of c is chosen to preserve structures with mean curvature $\frac{1}{\sigma}$, but not structures with mean curvature $\frac{2}{\sigma}$. A larger value of c is chosen for the Filament 3 video so that both structures are preserved.

5. Application to the Steiner problem

The numerical experiments and observations of the previous sections on the Allen–Cahn equation coupled with the skeletal term (4.1) lead us naturally to address the application to the Steiner problem in 3D. Recall that the Steiner problem consists in finding, for a given collection of points $a_0, \dots, a_N \in Q$, a compact connected set $K \subset Q$ containing all the a_i's and having minimal length. In other words, it amounts to solving the following minimization problem:

$$\min\left\{\mathcal{H}^1(K) \mid K \subset Q,\ K \text{ connected},\ \forall i,\ a_i \in K\right\}.$$

The numerical approximation of solutions to this problem is notoriously difficult, especially in dimension ≥ 3; see, for instance, [15–18,26,27,31,43,44]. The model we propose provides an effective and natural way to approximate these solutions in 3D (and actually even in higher dimensions, because the extension is straightforward).

5.1. A σ-thickened Steiner problem

We consider an approximation of the Steiner problem in 3D for the σ-tubular set $K_\sigma := \{x \in \mathbb{R}^3 \mid \operatorname{dist}(x, K) \leq \sigma\}$, which is the σ-thickening of K. We choose the thickening parameter σ to be small enough, as in Lemma 2.2, so that a minimal distance between the boundary of K_σ and its skeleton K is ensured.

It is clear that the length of K is approximated by the perimeter of K_σ in the sense that

$$\mathcal{P}(K_\sigma) \simeq 2\pi\sigma\mathcal{H}^1(K).$$

[3] https://plmbox.math.cnrs.fr/f/833b8a034cf143c68e30/ visited on 30 March 2026
[4] https://plmbox.math.cnrs.fr/f/bc7254ad02384e788cea/ visited on 30 March 2026

Moreover, the property that K contains all points a_i can be replaced by the *inclusion constraint*

$$\bigcup_{i=1}^{N} B(a_i,\sigma) \subset K_\sigma, \tag{5.1}$$

which means that K_σ contains all the balls $B(a_i,\sigma)$ of radius σ.

We now explain how to obtain a phase field approximation of the minimization problem

$$\min\Big\{\mathcal{H}^2(K_\sigma) \mid \bigcup_{i=1}^{N} B(a_i,\sigma) \subset K_\sigma \text{ and } \operatorname{dist}(\partial K_\sigma, \Sigma(K_\sigma)) \geq \sigma\Big\},$$

where $\Sigma(K_\sigma)$ is the skeleton of ∂K_σ.

5.2. Phase field approximation of the thickened Steiner problem

There is a natural way to approximate inclusion constraint (5.1) using phase fields (see [21]). This can be done by first introducing the function $u_{\text{in}}^\varepsilon$ defined by

$$u_{\text{in}}^\varepsilon(x) := q\Big(\frac{\operatorname{dist}(x, \cup_{i=1}^N\{a_i\}) - \widetilde{\sigma}}{\varepsilon}\Big),$$

where $\operatorname{dist}(x, \bigcup_{i=1}^N\{a_i\})$ denotes the distance function to the collection of all points a_i, q is the usual optimal profile associated with the double-well function, and $\widetilde{\sigma} > 0$. Inclusion constraint (5.1) can thus be implemented by considering the inequality constraint $u_{\text{in}}^\varepsilon \leq u^\varepsilon$. Indeed, it is not difficult to observe that

$$u_{\text{in}}^\varepsilon \leq u^\varepsilon \implies \bigcup_{i=1}^{N} B(a_i,\widetilde{\sigma}) \subset \big\{x; u^\varepsilon(x) \geq 0\big\}.$$

Therefore, we define recursively the sequence $\{u^n\}_{n\in\mathbb{N}}$ by $u^{n+1}(x) = \max(\widetilde{u}^{n+1}, u_{\text{in}}^\varepsilon(x))$, where

$$\widetilde{u}^{n+1} = (I_d - \delta_t(\Delta - \frac{\alpha}{\epsilon^2}I_d))^{-1}\Big(u^n - \delta_t\Big((1 + f_{u^n}^\sigma(x))\frac{W'(u^n)}{\varepsilon^2} - \frac{\alpha}{\epsilon^2}u^n\Big)\Big).$$

5.3. Numerical experiments

We define $Q = [-0.5, 0.5]^3$ and we use the following settings: $N = 2^7$, $\varepsilon = 2/N$, $h = \delta_t = \varepsilon^2$, $\sigma^2 = 0.1\varepsilon^2$, $c = 0.35\varepsilon N^3$, and $\widetilde{\sigma} = 0.02$.

The first example in Figure 8 represents the case where the a_i's are the vertices of a cube. The initial set is also a cube containing all nodes a_i. We show in Figure 8 approximate solutions at different times of the phase field flow.

We note that although the initial set is of dimension 3 (the initial cube), the stationary solution is close to a tubular thickening of a set of dimension 1 containing all the nodes a_i. We observe that this solution is very close to the real Steiner tree associated with the cube vertices; in particular, all the angles at each triple junction are equal to $2\pi/3$.

As a comparison, we consider in Figure 9 an example with 10 points randomly distributed in Q, which leads exactly to the same conclusion.

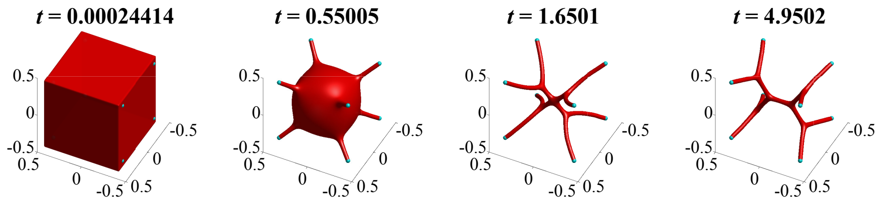

Figure 8. A Steiner tree associated with cube vertices: illustration of the approximate solutions at different times of the numerical flow. The red and blue interfaces are, respectively, the 0-level set of u^n and the set $\bigcup_{i=1}^N B(a_i, \widetilde{\sigma})$.

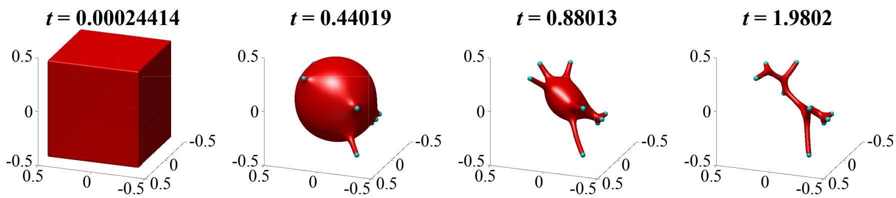

Figure 9. A Steiner tree associated with 10 points randomly chosen in Q: illustration of the approximate solutions at different times of the numerical flow. The red and blue interfaces are, respectively, the 0-level set of u^n and the set $\bigcup_{i=1}^N B(a_i, \widetilde{\sigma})$.

To get a better idea of the numerical flows computed with our model, videos (in .avi format) can be downloaded at the following addresses:

- Video of the flow of Figure 8: Approximation of the Steiner set of cube vertices.[5]
- Approximation of the Steiner tree associated with 50 randomly chosen points: Approximation of the Steiner set of 50 random points.[6]

6. Application to the Plateau problem

Our last numerical application is devoted to the celebrated Plateau problem. Recall that the Plateau problem was formulated by Lagrange in 1760 and consists in finding, for a given closed Jordan curve γ, a surface E in $\mathbb{R}^3$ with a (locally minimal) area such that the boundary of E coincides with γ. In other words, it amounts to solving the following minimization problem:

[5] https://plmbox.math.cnrs.fr/f/a0ea6869c4ca4a5a903a/ visited on 30 March 2026
[6] https://plmbox.math.cnrs.fr/f/01edbac59d534206a36d/ visited on 30 March 2026

$$\min\left\{\mathcal{H}^2(E),\ E \subset \Omega,\ \text{connected and such that } \partial E = \gamma\right\}.$$

Solutions to this problem are called minimal surfaces. Many numerical methods have been developed to approximate such surfaces: parametric approaches involving tools from discrete or continuous differential geometry [30, 37, 37, 39, 40, 56, 62, 64], level set methods [25,29], or phase field models [27] that provide particularly suitable numerical approximations, but restricted to oriented surfaces.

6.1. A σ-thickened Plateau problem

We consider a σ-thickened minimal surface problem for the σ-tubular thickening of a given Jordan curve γ,

$$\gamma_\sigma := \left\{x \mid \mathrm{d}(x,\gamma) \leq \sigma\right\},$$

by considering the following minimization problem:

$$\min\left\{\mathcal{P}(E_\sigma) + \frac{c}{\sigma}\mathcal{H}^3(E_\sigma) \mid E_\sigma \subset \mathbb{R}^3 \text{connected and } \gamma_\sigma \subset E_\sigma\right\},$$

where $\mathcal{H}^3(E_\sigma)$ stands for the volume of E_σ. Here, with σ chosen sufficiently small, the volume term is included to constrain E_σ to have a thickness of order σ, provided there exists a connected set E such that

$$E_\sigma \simeq \{x \in \mathbb{R}^3; \mathrm{dist}(x, E) \leq \sigma\} \quad \text{and} \quad \mathcal{P}(E_\sigma) \simeq 2\mathcal{H}^2(E).$$

Figure 10 shows what may happen if this volume term is not used: it is not possible to get in the limit a “thin” volume that approximates a minimal surface.

As before, from an initial connected set, the connectedness property is preserved thanks to the skeletal term in the penalized mean curvature flow.

Remark 6.1. Unlike the thickened Plateau problem, there is no need to penalize volume in the thickened Steiner problem. The reason for this is simple: in the Steiner problem, the constraints on the vertices, combined with a property of minimizing the surface area of the flow, lead to a natural reduction in volume to achieve a final tubular set.

6.2. Phase-field approximation of the thickened Plateau problem

Similarly to the thickened Steiner problem, let us define $u^\varepsilon_{\text{in}}$ as

$$u^\varepsilon_{\text{in}}(x) = q\left(\frac{\mathrm{dist}(x,\gamma_{\widetilde{\sigma}})}{\varepsilon}\right),$$

where $\widetilde{\sigma} > 0$, and consider the sequence $(u^n)_n$ by combining a perturbed Allen–Cahn equation with an additional inclusion constraint—that is, we compute

$$u^{n+1}(x) = \max(\widetilde{u}^{n+1}, u^\varepsilon_{\text{in}}),$$

where $\widetilde{u}^{n+1}$ is an approximation of v at time δ_t, where v is solution of the flow

$$\begin{cases} \partial_t v(x,t) = \Delta v(x,t) - \dfrac{W'(v(x,t))}{\varepsilon^2}(1 + f^{\sigma}_{u^n}(x)) + \dfrac{c_{\text{volume}}}{\varepsilon\sigma}\sqrt{2W(u^n)}, \\ v(\cdot,0) = u^n. \end{cases}$$

More precisely, similarly to the Steiner problem, we use the following numerical approximation in practice:

$$\widetilde{u}^{n+1} = \left(I_d - \delta_t\left(\Delta - \frac{\alpha}{\epsilon^2}I_d\right)\right)^{-1}\left(u^n - \delta_t\left((1 + f^{\sigma}_{u^n}(x))\frac{W'(u^n)}{\varepsilon^2} - \frac{\alpha}{\epsilon^2}u^n\right)\right. \\ \left. + \frac{c_{\text{volume}}}{\varepsilon\sigma}\sqrt{2W(u^n)},\right).$$

6.3. Numerical experiments

We set $Q = [-0.5, 0.5]^3$, $N = 2^7$, $\varepsilon = 2/N$, $h = \delta_t = \varepsilon^2$, $\sigma^2 = 0.1\varepsilon^2$, $c = 0.35\varepsilon N^3$, and $\widetilde{\sigma} = 0.02$.

In Figure 10, we show the solution obtained at different times using the parameter $c_{\text{volume}} = 0$. With this setting, the volume is not penalized over the iterations. We observe that the final stationary set has not the right form in the sense that its thickness is not of size $\widetilde{\sigma}$, that is, the set cannot be associated with a minimal 2D surface. This experiment shows all the interest to penalize the volume in our computations.

All subsequent numerical experiments in this section are therefore performed with the setting $c_{\text{volume}} = 1$.

The main purpose of Figure 11 is to illustrate the influence on the result of the topology of the initial set. The two lines correspond to two distinct initial configurations, and the images show the evolving approximate solutions at different times. Our model appears to be capable of approximating various minimal surfaces associated with a given curve. The topology of the limit surface depends naturally on the choice of the initial set.

Figure 12 illustrates the ability of our method to approximate non-orientable minimal surfaces and minimal surfaces with triple line singularities. The first line shows an example of a non-smooth (approximate) minimal surface, while the second gives an approximation of a Möbius strip. Note that in the latter case, we start from an initial connected set given by a cube with a cylindrical hole.

To get a better idea of numerical flows computed with our model, videos (in .avi format) can be downloaded at the following addresses:

- Video of the flow illustrated in Figure 11, right: An (approximate) Plateau solution.[7]
- Approximation of a Möbius strip with a singularity line: A singular (approximate) Möbius strip.[8]

[7] https://plmbox.math.cnrs.fr/f/8146f9724e564893b1e2/ visited on 30 March 2026
[8] https://plmbox.math.cnrs.fr/f/035ab68314754a4897c6/ visited on 30 March 2026

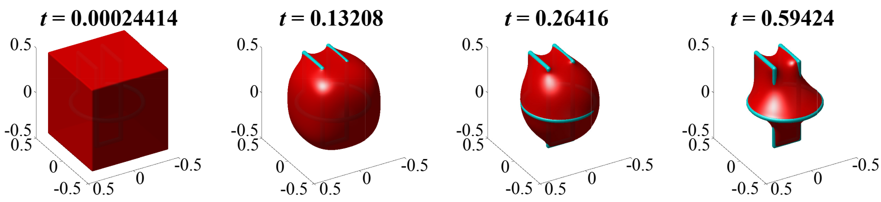

Figure 10. Numerical illustration of the gradient flow for the thickened Plateau problem without volume penalization: the stationary shape is not at all close to a minimal surface

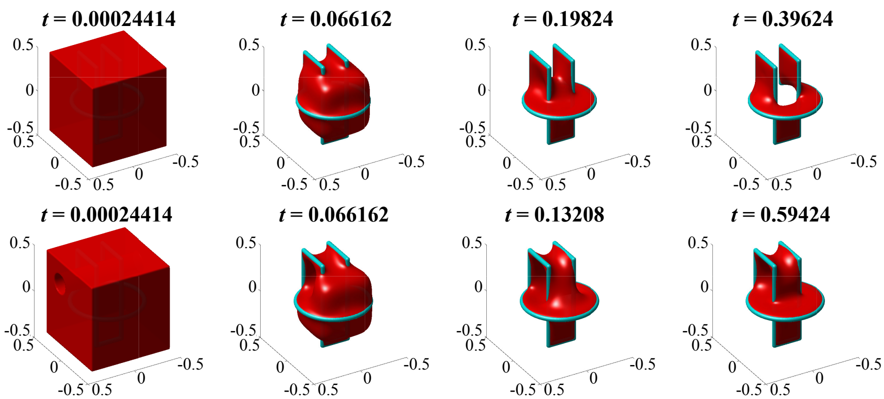

Figure 11. Numerical approximation of (at least local) solutions to the Plateau problem using our phase field method. The experiment illustrates the influence on the result of the initial set's topology. Each line shows the numerical solution at different times starting from a distinct initial configuration.

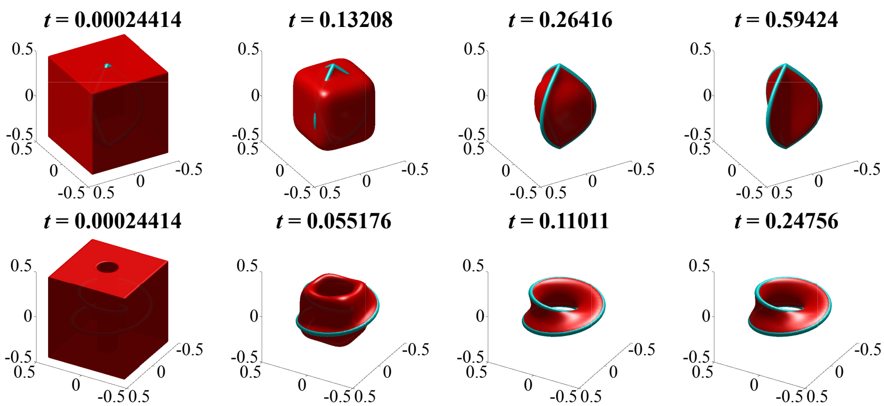

Figure 12. Numerical approximation of (at least local) solutions to the Plateau problem using the proposed flow. First line: convergence to a minimal surface with a triple line singularity. Second line: convergence to a Möbius strip, an example of non-orientable surface that our model can compute.

- An hybrid solution combining a Steiner set and a minimal surface: A Steiner-Plateau hybrid solution.[9]

Funding. The authors acknowledge support from the French National Research Agency (ANR) under grants ANR-18-CE05-0017 (project BEEP) and ANR-19-CE01-0009-01 (project MIMESIS-3D). Part of this work was also supported by the LABEX MILYON (ANR-10-LABX-0070) of Université de Lyon, within the program "Investissements d'Avenir" (ANR-11-IDEX-0007) operated by the French National Research Agency (ANR), and by the European Union Horizon 2020 research and innovation programme under the Marie Sklodowska-Curie grant agreement No 777826 (NoMADS).

References

[1] S. M. Allen and J. W. Cahn. A microscopic theory for antiphase boundary motion and its application to antiphase domain coarsening. *Acta Metall.*, **27** (1979), 1085–1095

[2] S. J. Altschuler, Singularities of the curve shrinking flow for space curves. *J. Differential Geom.* **34** (1991), no. 2, 491–514 Zbl 0754.53006 MR 1131441

[3] L. Ambrosio, Geometric evolution problems, distance function and viscosity solutions. In *Calculus of Variations and Partial Differential Equations*, pp. 5–93, Springer, Berlin, 2000 Zbl 0956.35002 MR 1757696

[4] L. Ambrosio, N. Fusco, and D. Pallara, *Functions of Bounded Variation and Free Discontinuity Problems*. Oxford Math. Monogr., The Clarendon Press, Oxford University Press, New York, 2000 Zbl 0957.49001 MR 1857292

[5] L. Ambrosio and C. Mantegazza, Curvature and distance function from a manifold. *J. Geom. Anal.* **8** (1998), 723–748 Zbl 0941.53009 MR 1731060

[6] L. Ambrosio and H. M. Soner, Level set approach to mean curvature flow in arbitrary codimension. *J. Differential Geom.* **43** (1996), no. 4, 693–737 Zbl 0868.35046 MR 1412682

[7] L. Ambrosio and H. M. Soner, A measure-theoretic approach to higher codimension mean curvature flows. *Ann. Sc. Norm. Super. Pisa, Cl. Sci., IV. Ser.* **25** (1997), no. 1–2, 27–49 Zbl 1043.35136 MR 1655508

[8] J. W. Barrett, H. Garcke, and R. Nürnberg, Numerical approximation of gradient flows for closed curves in $\mathbb{R}^d$. *IMA J. Numer. Anal.* **30** (2010), no. 1, 4–60 Zbl 1185.65027 MR 2580546

[9] J. W. Barrett, H. Garcke, and R. Nürnberg, Parametric approximation of isotropic and anisotropic elastic flow for closed and open curves. *Numer. Math.* **120** (2012), no. 3, 489–542 Zbl 1242.65188 MR 2890298

[10] G. Bellettini, *Lecture notes on mean curvature flow, barriers and singular perturbations*. Appunti. Sc. Norm. Super. Pisa (N. S.) [Lecture Notes. Scuola Normale Superiore di Pisa (New Series)] 12, Edizioni della Normale, Pisa, 2013 Zbl 1312.53002 MR 3155251

[11] G. Bellettini and M. Novaga, A result on motion by mean curvature in arbitrary codimension. *Differential Geom. Appl.* **11** (1999), no. 3, 205–220 Zbl 0959.35085 MR 1726537

[9] https://plmbox.math.cnrs.fr/f/9e6ca67821214f51ba9a/ visited on 30 March 2026

[12] G. Bellettini and M. Paolini, Quasi-optimal error estimates for the mean curvature flow with a forcing term. *Differential Integral Equations* **8** (1995), no. 4, 735–752 Zbl 0820.49019 MR 1306590

[13] F. Bethuel, G. Orlandi, and D. Smets, Convergence of the parabolic Ginzburg-Landau equation to motion by mean curvature. *Ann. of Math. (2)* **163** (2006), no. 1, 37–163 Zbl 1103.35038 MR 2195132

[14] T. Binz and B. Kovács, A convergent finite element algorithm for mean curvature flow in arbitrary codimension. *Interfaces Free Bound.* **25** (2023), no. 3, 373–400 Zbl 07761250 MR 4642018

[15] M. Bonafini, G. Orlandi, and É. Oudet, Variational approximation of functionals defined on 1-dimensional connected sets: the planar case. *SIAM J. Math. Anal.* **50** (2018), no. 6, 6307–6332 Zbl 1404.49006 MR 3890784

[16] M. Bonafini and É. Oudet, A convex approach to the Gilbert-Steiner problem. *Interfaces Free Bound.* **22** (2020), no. 2, 131–155 Zbl 1448.49019 MR 4122481

[17] M. Bonnivard, E. Bretin, and A. Lemenant, Numerical approximation of the Steiner problem in dimension 2 and 3. *Math. Comp.* **89** (2020), no. 321, 1–43 Zbl 1447.65055 MR 4011534

[18] M. Bonnivard, A. Lemenant, and F. Santambrogio, Approximation of length minimization problems among compact connected sets. *SIAM J. Math. Anal.* **47** (2015), no. 2, 1489–1529 Zbl 1319.49075 MR 3337998

[19] M. Brassel and E. Bretin, A modified phase field approximation for mean curvature flow with conservation of the volume. *Math. Methods Appl. Sci.* **34** (2011), no. 10, 1157–1180 Zbl 1235.49082 MR 2838769

[20] E. Bretin, A. Chambolle, and S. Masnou. A Cahn–Hilliard-Willmore phase field model for non-oriented interfaces. To appear in *Interfaces Free Bound*. 2025, arXiv:2412.15926

[21] E. Bretin, F. Dayrens, and S. Masnou, Volume reconstruction from slices. *SIAM J. Imaging Sci.* **10** (2017), no. 4, 2326–2358 Zbl 1408.49044 MR 3738845

[22] E. Bretin, R. Denis, S. Masnou, and G. Terii, Learning phase field mean curvature flows with neural networks. *J. Comput. Phys.* **470** (2022), article no. 111579 Zbl 1562.65144 MR 4483340

[23] E. Bretin and V. Perrier, Phase field method for mean curvature flow with boundary constraints. *ESAIM Math. Model. Numer. Anal.* **46** (2012), no. 6, 1509–1526 Zbl 1272.65057 MR 2996338

[24] E. Carlini, M. Falcone, and R. Ferretti, A semi-Lagrangian scheme for the curve shortening flow in codimension-2. *J. Comput. Phys.* **225** (2007), no. 2, 1388–1408 Zbl 1255.65157 MR 2349186

[25] T. Cecil, A numerical method for computing minimal surfaces in arbitrary dimension. *J. Comput. Phys.* **206** (2005), no. 2, 650–660 Zbl 1070.65048 MR 2143330

[26] A. Chambolle, L. A. D. Ferrari, and B. Merlet, A phase-field approximation of the Steiner problem in dimension two. *Adv. Calc. Var.* **12** (2019), no. 2, 157–179 Zbl 1412.49085 MR 3935855

[27] A. Chambolle, L. A. D. Ferrari, and B. Merlet, Variational approximation of size-mass energies for k-dimensional currents. *ESAIM Control Optim. Calc. Var.* **25** (2019), article no. 43 Zbl 1437.49061 MR 4009414

[28] X. Chen, Generation and propagation of interfaces for reaction-diffusion equations. *J. Differential Equations* **96** (1992), no. 1, 116–141 Zbl 0765.35024 MR 1153311

[29] D. L. Chopp, Computing minimal surfaces via level set curvature flow. *J. Comput. Phys.* **106** (1993), no. 1, 77–91 Zbl 0786.65015 MR 1214016

[30] C. Coppin and D. Greenspan, A contribution to the particle modeling of soap films. *Appl. Math. Comput.* **26** (1988), no. 4, 315–331 Zbl 0651.65008 MR 942778

[31] C. D'Ambrosio, M. Fampa, J. Lee, and S. Vigerske. On a nonconvex MINLP formulation of the Euclidean Steiner tree problem in n-space. In *Experimental Algorithms: 14th International Symposium, SEA 2015, Paris, France, June 29 – July 1, 2015, Proceedings*, pp. 122-–133. Lect. Notes Comp. Sci. 9125, Springer, 2015.

[32] P. de Mottoni and M. Schatzman, Geometrical evolution of developed interfaces. *Trans. Amer. Math. Soc.* **347** (1995), no. 5, 1533–1589 Zbl 0840.35010 MR 1672406

[33] E. De Giorgi. Congetture riguardanti barriere, superfici minime, movimenti secondo la curvatura. Dattiloscritto, Lecce, 4 novembre 1993.

[34] K. Deckelnick and G. Dziuk, On the approximation of the curve shortening flow. In *Calculus of variations, applications and computations (Pont-à-Mousson, 1994)*, pp. 100–108, Pitman Res. Notes Math. Ser. 326, Longman Sci. Tech., Harlow, 1995 Zbl 0830.65096 MR 1419337

[35] M. P. do Carmo, *Differential geometry of curves and surfaces*. Prentice-Hall, Englewood Cliffs, NJ, 1976 Zbl 0326.53001 MR 394451

[36] W. Dörfler and R. Nürnberg, Discrete gradient flows for general curvature energies. *SIAM J. Sci. Comput.* **41** (2019), no. 3, A2012–A2036 Zbl 1434.65178 MR 3968254

[37] J. Douglas, A method of numerical solution of the problem of Plateau. *Ann. of Math. (2)* **29** (1927/28), no. 1–4, 180–188 Zbl 54.0509.02 MR 1502829

[38] G. Dziuk, Convergence of a semi-discrete scheme for the curve shortening flow. *Math. Models Methods Appl. Sci.* **4** (1994), no. 4, 589–606 Zbl 0811.65112 MR 1291140

[39] G. Dziuk and J. E. Hutchinson, The discrete Plateau problem: algorithm and numerics. *Math. Comp.* **68** (1999), no. 225, 1–23 Zbl 0913.65062 MR 1613695

[40] G. Dziuk and J. E. Hutchinson, The discrete Plateau problem: convergence results. *Math. Comp.* **68** (1999), no. 226, 519–546 Zbl 1043.65126 MR 1613699

[41] K. Ecker, *Regularity theory for mean curvature flow*. Progr. Nonlinear Differential Equations Appl. 57, Birkhäuser, Boston, MA, 2004 Zbl 1058.53054 MR 2024995

[42] O. Hershkovits, Mean curvature flow of arbitrary co-dimensional Reifenberg sets. *Calc. Var. Partial Differential Equations* **57** (2018), no. 6, article no. 148 Zbl 1400.53055 MR 3858831

[43] D. Juhl, D. Warme, P. Winter, and M. Zachariasen. The GeoSteiner software package for computing Steiner trees in the plane: an updated computational study. *Math. Program. Comput.* **10** (2018), no. 4, 487–532 Zbl 1411.90225 MR 3863702

[44] R. M. Karp, Reducibility among combinatorial problems. In *Complexity of computer computations (Proc. Sympos., IBM Thomas J. Watson Res. Center, Yorktown Heights, N.Y., 1972)*, pp. 85–103, The IBM Research Symposia Series, Plenum, New York-London, 1972 Zbl 1467.68065 MR 378476

[45] T. Laux and N. K. Yip, Analysis of diffusion generated motion for mean curvature flow in codimension two: a gradient-flow approach. *Arch. Ration. Mech. Anal.* **232** (2019), no. 2, 1113–1163 Zbl 1411.53050 MR 3925538

[46] C. Mantegazza, *Lecture notes on mean curvature flow*. Progr. Math. 290, Birkhäuser, Basel, 2011 Zbl 1230.53002 MR 2815949

[47] C. Mantegazza and A. C. Mennucci, Hamilton-Jacobi equations and distance functions on Riemannian manifolds. *Appl. Math. Optim.* **47** (2003), no. 1, 1–25 Zbl 1048.49021 MR 1941909

[48] K. Mikula and J. Urbán, A new tangentially stabilized 3D curve evolution algorithm and its application in virtual colonoscopy. *Adv. Comput. Math.* **40** (2014), no. 4, 819–837 Zbl 1296.65030 MR 3240215

[49] L. Modica and S. Mortola, Un esempio di Γ^--convergenza. *Boll. Un. Mat. Ital. B (5)* **14** (1977), no. 1, 285–299 Zbl 0356.49008 MR 445362

[50] L. Mugnai and M. Röger, Convergence of perturbed Allen-Cahn equations to forced mean curvature flow. *Indiana Univ. Math. J.* **60** (2011), no. 1, 41–75 Zbl 1316.35150 MR 2952409

[51] P. Pozzi, Anisotropic curve shortening flow in higher codimension. *Math. Methods Appl. Sci.* **30** (2007), no. 11, 1243–1281 Zbl 1122.65081 MR 2334978

[52] P. Pozzi, Anisotropic mean curvature flow for two-dimensional surfaces in higher codimension: a numerical scheme. *Interfaces Free Bound.* **10** (2008), no. 4, 539–576 Zbl 1158.65076 MR 2465273

[53] Y. Qi and G.-F. Zheng, Convergence of solutions of the weighted Allen-Cahn equations to Brakke type flow. *Calc. Var. Partial Differential Equations* **57** (2018), no. 5, article no. 133 Zbl 1428.35180 MR 3844514

[54] S. J. Ruuth, Efficient algorithms for diffusion-generated motion by mean curvature. *J. Comput. Phys.* **144** (1998), no. 2, 603–625 Zbl 0946.65093 MR 1638032

[55] S. J. Ruuth, B. Merriman, J. Xin, and S. Osher, Diffusion-generated motion by mean curvature for filaments. *J. Nonlinear Sci.* **11** (2001), no. 6, 473–493 Zbl 1037.35033 MR 1871280

[56] H. Schumacher and M. Wardetzky, Variational convergence of discrete minimal surfaces. *Numer. Math.* **141** (2019), no. 1, 173–213 Zbl 1408.49039 MR 3903206

[57] L. Simon, *Lectures on geometric measure theory*. Proc. Centre Math. Anal. Austral. Nat. Univ. 3, Australian National University, Centre for Mathematical Analysis, Canberra, 1983 Zbl 0546.49019 MR 756417

[58] D. Slepčev, On level-set approach to motion of manifolds of arbitrary codimension. *Interfaces Free Bound.* **5** (2003), no. 4, 417–458 Zbl 1040.35126 MR 2031465

[59] K. Smoczyk, Mean curvature flow in higher codimension: introduction and survey. In *Global differential geometry*, pp. 231–274, Springer Proc. Math. 17, Springer, Heidelberg, 2012 Zbl 1247.53004 MR 3289845

[60] J. Taylor, *Crystals, in equilibrium and otherwise*. AMS-MAA Joint Lecture Ser., American Mathematical Society, Providence, RI, 1990 Zbl 0776.65002 MR 1109716

[61] Y. Tonegawa, *Brakke's mean curvature flow*. SpringerBriefs Math., Springer, Singapore, 2019 Zbl 1448.49002 MR 3930606

[62] H.-J. Wagner, A contribution to the numerical approximation of minimal surfaces. *Computing* **19** (1977/78), no. 1, 35–58 Zbl 0374.49021 MR 458923

[63] M.-T. Wang, Long-time existence and convergence of graphic mean curvature flow in arbitrary codimension. *Invent. Math.* **148** (2002), no. 3, 525–543 Zbl 1039.53072 MR 1908059

[64] S. Wang and A. Chern. Computing minimal surfaces with differential forms. *ACM Trans. Graph.*, **40** (2021), no. 4, article no. 113, 1–14

Received 4 June 2024; revised 7 October 2025.

Elie Bretin
INSA Lyon, 20 avenue Albert Einstein, 69621 Villeurbanne; CNRS, DR7 - Délégation Rhône Auvergne, 2 avenue Albert Einstein, B.P. 1335, 69609 Villeurbanne; École Centrale de Lyon, 36

avenue Guy de Collongue, 69134 Écully; Université Claude Bernard Lyon 1, 43 boulevard du 11 novembre 1918, 69622 Villeurbanne; Université Jean Monnet, Maison de l'université, 10 rue Tréfilerie – CS 82301, 42023 Saint-Etienne; Institut Camille Jordan (ICJ) UMR5208, 43 boulevard du 11 novembre 1918, 69622 Villeurbanne, France; elie.bretin@insa-lyon.fr
Author IDs: MR 932768 ORCID 0000-0003-1319-7538

Chih-Kang Huang
Université Claude Bernard Lyon 1, 43 boulevard du 11 novembre 1918, 69622 Villeurbanne; CNRS, DR7 - Délégation Rhône Auvergne, 2 avenue Albert Einstein, B.P. 1335, 69609 Villeurbanne; École Centrale de Lyon, 36 avenue Guy de Collongue, 69134 Écully; INSA Lyon, 20 avenue Albert Einstein, 69621 Villeurbanne; Université Jean Monnet, Maison de l'université, 10 rue Tréfilerie – CS 82301, 42023 Saint-Etienne; Institut Camille Jordan (ICJ) UMR5208, 43 boulevard du 11 novembre 1918, 69622 Villeurbanne, France;
chih-kang.huang@hotmail.com, chih-kang.huang@inria.fr
Author IDs: ORCID 0009-0005-3946-910X

Simon Masnou
Université Claude Bernard Lyon 1, 43 boulevard du 11 novembre 1918, 69622 Villeurbanne; CNRS, DR7 - Délégation Rhône Auvergne, 2 avenue Albert Einstein, B.P. 1335, 69609 Villeurbanne; École Centrale de Lyon, 36 avenue Guy de Collongue, 69134 Écully; INSA Lyon, 20 avenue Albert Einstein, 69621 Villeurbanne; Université Jean Monnet, Maison de l'université, 10 rue Tréfilerie – CS 82301, 42023 Saint-Etienne; Institut Camille Jordan (ICJ) UMR5208, 43 boulevard du 11 novembre 1918, 69622 Villeurbanne, France;
masnou@math.univ-lyon1.fr
Author IDs: MR 641699 ORCID 0000-0003-3664-3262

Licensed under the Creative Commons Attribution 4.0 International License CC BY 4.0 (https://creativecommons.org/licenses/by/4.0/), which permits use, sharing, adaptation, and redistribution with appropriate credit, a link to the license, and indication of changes.